UNIVERSITY OF SOUTHAMPTON
School Of Engineering Sciences, Ship Science

AN INVESTIGATION INTO THE CAPABILITIES OF COMPUTATIONAL FLUID DYNAMICS IN SAIL PERFORMANCE PREDICTION

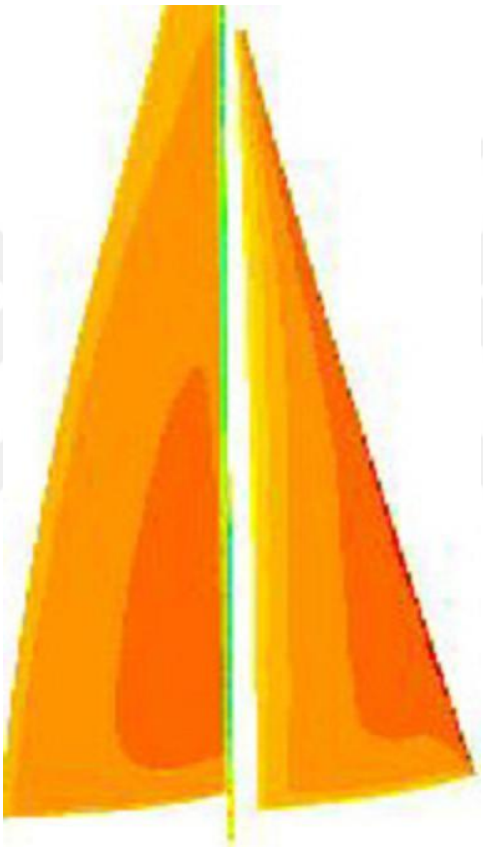

MSc Thesis
by Ahmet Ziya SAYDAM
October 2005

UNIVERSITY OF SOUTHAMPTON

ABSTRACT

FACULTY OF ENGINEERING AND APPLIED SCIENCE

SCHOOL OF ENGINEERING SCIENCES, SHIP SCIENCE

Master of Science

AN INVESTIGATION INTO THE CAPABILITIES OF COMPUTATIONAL FLUID DYNAMICS IN SAIL PERFORMANCE PREDICTION

by Ahmet Ziya Saydam

Wind tunnel experiments have always been an important part of the sailing yacht design process, in order to estimate the performance of the yachts. Their high cost, need for different models for different cases and scientific difficulties about simulating a realistic sailing environment have led computational methods to be used for performance estimates of sailing yachts. As yet, computational methods have not fully replaced experiments; they are generally being used for validation or academic purposes. This project aims to investigate the capabilities of CFD in terms of sail performance prediction. RANS solvers will be used for performance estimates and experimental results will be compared to numerically obtained results in order to assess the possibility of RANS codes being a cost effective replacement for wind tunnel experiments.

CONTENTS

APPENDICES

LIST OF FIGURES

LIST OF TABLES

NOMENCLATURE

AR_E	Effective Aspect Ratio
C	Wind Tunnel Cross Sectional Area
C_D	Drag Coefficient
C_{Dc}	Drag Coefficient Corrected for Wake Blockage
C_{Di}	Induced Drag Coefficient
C_{Du}	Drag Coefficient not Corrected for Wake Blockage
CFD	Computational Fluid Dynamics
C_L	Lift Coefficient
C_P	Pressure Coefficient
CPU	Central Processor Unit
D	Drag Force
D_F	Drive Force
g	Gravitational Acceleration
h	Static Head
H_F	Heel Force
L	Lift Force
m	Wake Blockage Correction Ratio
NACA	National Advisory Committee for Aeronautics
P	Pressure
q	Dynamic Head
RANS	Reynolds Averaged Navier Stokes
S	Sectional Area of Wind Tunnel
V	Velocity
VPP	Velocity Prediction Program
Y+	Wall Distance Unit
α	Angle of Attack
β	Apparent Wind Angle
ρ	Density

ACKNOWLEDGEMENTS

The author would like to thank Prof. Philip Wilson and Dr. Mingyi Tan for their continued support and supervision; Dr. Neil Bressloff and Ms. Nici Hoyle for their assistance with CFD analysis; Mr. Ian Campbell and Dr. Martyn Prince for their help within all aspects of the project; Dr. Stuart Wilkinson for his support and consultancy about his experiments and Mr. Mike Tudor-Pole for his assistance in the wind tunnel experiments.

1. INTRODUCTION

Wind tunnel experimenting is one of the most useful tools in sailing yacht design. Especially with the testing techniques developed during the last century, mainly for aerospace research, useful information can be gained from wind tunnel testing in both the pre-design and the detail design stages.

Even though the aerospace related testing techniques might be incorporated into sailing yacht testing to get useful data, this is limited to a certain extent owing to the major differences in the analogies associated between the two. Problems associated with scaling difficulties in terms of Reynolds Numbers, simulation of the wind gradient and twist, simulating the air sea interface and the boundary layer between the two, material considerations associated with matching the structural characteristics of the model and the yacht rigs, the need to build different rig and hull models for different configurations have always been obstacles for researchers and designers of sailing yachts.

A substantial amount of academic and industrial research has been done to overcome the previously stated problems; however a limited amount has been published due to confidentiality reasons. This leads to the fact that there is no consensus about the methodology of wind tunnel testing of sailing yachts in terms of the mentioned problematic issues. Companies, academic institutions and researchers have evolved their own techniques after gaining considerable experience.

Recently, computational fluid dynamics methods have gained popularity in the academic based research field. Following the development in the computer industry in the past decade, the availability of powerful computational resources has given momentum to the usage of computational fluid dynamics methods in the academic research. Quite considerable amount of work has been done since then which include development of new techniques and softwares which encouraged the designers to incorporate the computational fluid dynamics methods into the design of sailing yachts.

The incorporation of computational fluid dynamics methods into the design process of sailing yachts has since been problematic due to several general reasons. Mainly, the requirement of

highly skilled engineers is one of the biggest obstacles. In addition, the highly time consuming nature of these methods makes them ineffective for usage in a design office environment.

Apart from the general problems associated with these methods, particular problems regarding sailing yacht design problem exist. The most challenging of these is the estimation of flying sail shape. Even methods have been developed aiming to couple a structural finite element code with a computational fluid dynamics code mainly by sail builders; they have not been developed to the extent required by the industry. It is stated in reference 1 that "this method will help to expedite the optimisation of sail design in providing a close link between realistic full scale wind conditions and sails, in particular their change in sail shape due to the sail material properties, the pressure magnitude, the distribution of pressure on the sails and due to the sail trim." It is further stated that the developed VWT (Virtual Wind Tunnel) will have mast, boom and the hull after further development. Also, it will be linked to a VPP later on.

Another peculiar problem is the requirement of high number of simulations in order to fully assess the performance of the yacht in all aspects. All these simulations demand different grids, different solver settings and they are highly time consuming.

As yet these challenges are not overcome and as a result computational fluid dynamics methods can not be a cost effective replacement for experiments. Wind tunnel experiments are still the major tool for assessing a yacht's performance. However, computational methods are integrated to the experiments in many ways in order to reduce costs of the experiments. First of all, initial computational assessments might be made on different configurations within reasonable accuracy that would not demand high computational resources and time for comparison. This is something that can not be done easily in wind tunnels due to the requirement of different models for different configurations. Also, computational methods can be a useful tool for validation of the experiments and also for visualisation purposes such as streamline monitoring and so on.

1.1 Aims and Objectives

The aim of this project is to investigate the capabilities of computational fluid dynamics in terms of sail performance prediction. A wind tunnel experiment on a one metre boat's sailing rig will be made to provide data for usage by the one metre class community which will comprise of assessing the effect of aerodynamic deck fairing on the boat's performance, making a comparison between running goose winged and running on the same gybe

conditions and assessing the effect of sheeting and twist in upwind performance. These tasks will be approached with the relevant theoretical methods presented for obtaining the optimum sailing points for various sailing conditions and further analysis will be made on the data. Also, scaling difficulties will be discussed throughout the report with presentation of different scaling methods used in sailing yacht wind tunnel investigations and evaluations will be made with particular emphasis in uncertainties associated with them mainly in terms of Reynolds number similarity, drag breakdown and lift modifications. The data will be scaled up to a pre determined scale and CFD calculations made on full scale will be compared with the scaled wind tunnel data to see the differences. In order to get reliable results from the 3-D CFD calculations, extensive 2-D calculations will be made for the validation of the experiment made by Wilkinson at the University of Southampton wind tunnel which is based on simulations of a 2-D extruded sail like foil sections with mast attachments. Throughout the 2-D calculations, solver settings, turbulence models and the necessary user based parameters will be varied to get the closest results to the experiments and most importantly a grid independence study will be made. This information will then be used in 3-D calculations. The results obtained from the 3-D calculations will be used to make comparisons with the experiments and the agreement between the two will be assessed.

2. THEORETICAL BACKGROUND

2.1 Force Breakdown of Sail Rigs

A sailing yacht operates at the boundary where air and water intersect; the sails, rig and the above water part of the hull are immersed in air and the underwater part of the hull is immersed in water. A yacht sailing at a constant speed in calm water experiences two forces due to the existence of the two fluids; the aerodynamic force is due to the airflow around the sails and the hydrodynamic force is due to motion in water. In calm water at constant speed, these forces balance, they are equal in magnitude and opposite in direction. [2]

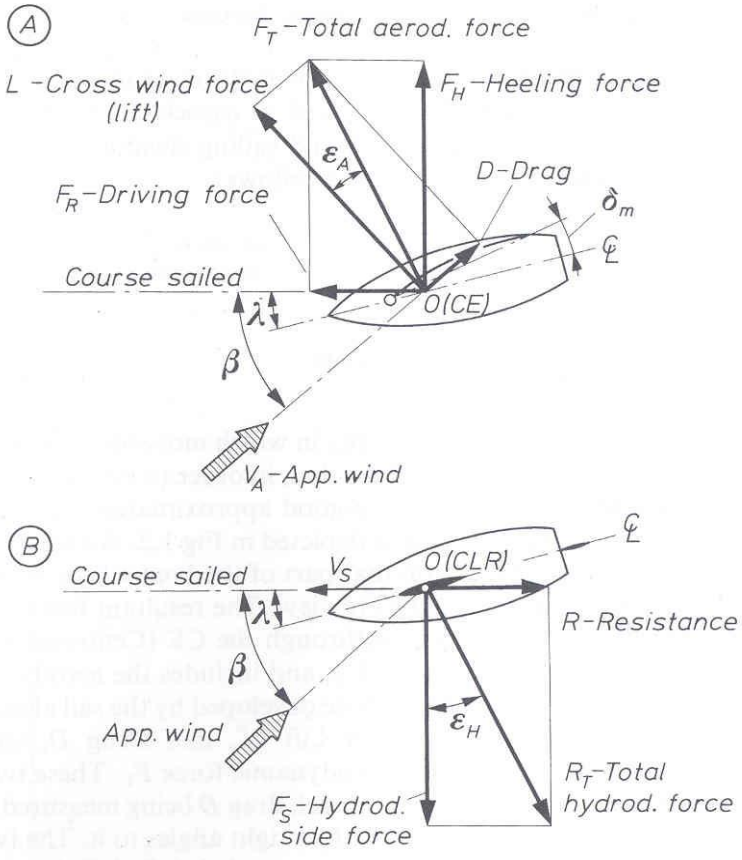

Figure 2.1

The sails experience the apparent wind, which is the vector sum of the true wind and wind due to the yacht's motion. Figure 2.1 shows that the total aerodynamic force can be resolved into lift which is perpendicular in direction to the apparent wind and drag which acts at the same direction as apparent wind. [3] This axis system is named wind axes. For convenience, by the appropriate translation these forces can also be expressed as driving force and heeling force on the space axes which is a right hand orthogonal axis system in line with the track of the yacht.[2]

There are two main components of the hydrodynamic force acting on the hull which are the resistance and the side force. These forces, as seen on figure 2.1 act along the space axis.

In order for the hull to produce side force, the keel has to have an angle of attack to the flow which is named the leeway angle. While the hull is producing side force, the angle between the heading of the yacht (in line with the body axis) and the track of the yacht (in line with the space axis) is equal to the leeway angle.

2.2 Aerodynamics of Sails

2.2.1 Flow Around Sails

The treatment of the mechanics of air flow around upwind sails is analogous to that of other conventional aerofoils such as aircraft wings or turbine blades that aim to generate a required lift force while creating the minimum drag possible.

Bernoulli's Equation

Sails operate immersed in air; due to the oncoming air flow, pressure acts along the sails on both sides. In order to better understand the physics of the flow around wing sections, Bernoulli's equation is a useful tool. Bernoulli states that the total pressure around a streamline is constant under the assumptions that the fluid is inviscid and incompressible. [4]

$$P + \tfrac{1}{2} \rho V^2 + \rho g h = \text{constant}$$

When the approaching flow encounters a sail, a stagnation point occurs near the leading edge that divides the flow into two parts. If the flow is in line with the sail, the pressure distributions along the windward and leeward sides of the sail are the same. When there is an angle of attack, the flow in the windward and leeward sides become asymmetric. The flow on the leeward side of the sail has to negotiate a higher curvature due to the angle of attack present. This results in speeding up of the flow on the leeward side. Due to Bernoulli's principle, this accelerated air results in lower pressure than the slower windward side. This small pressure difference becomes measurable when integrated along the whole sail area and it is the main source of lift production. A convenient way to express the pressure difference is the usage of the Pressure Coefficient, Cp.[4]

$$Cp=1-(q/v)^2$$

Figure 2.2 shows a typical pressure coefficient distribution plot. It shows how the air is accelerated on the leeward side and how the addition of the foresail accelerates the flow known as the slot effect. [5]

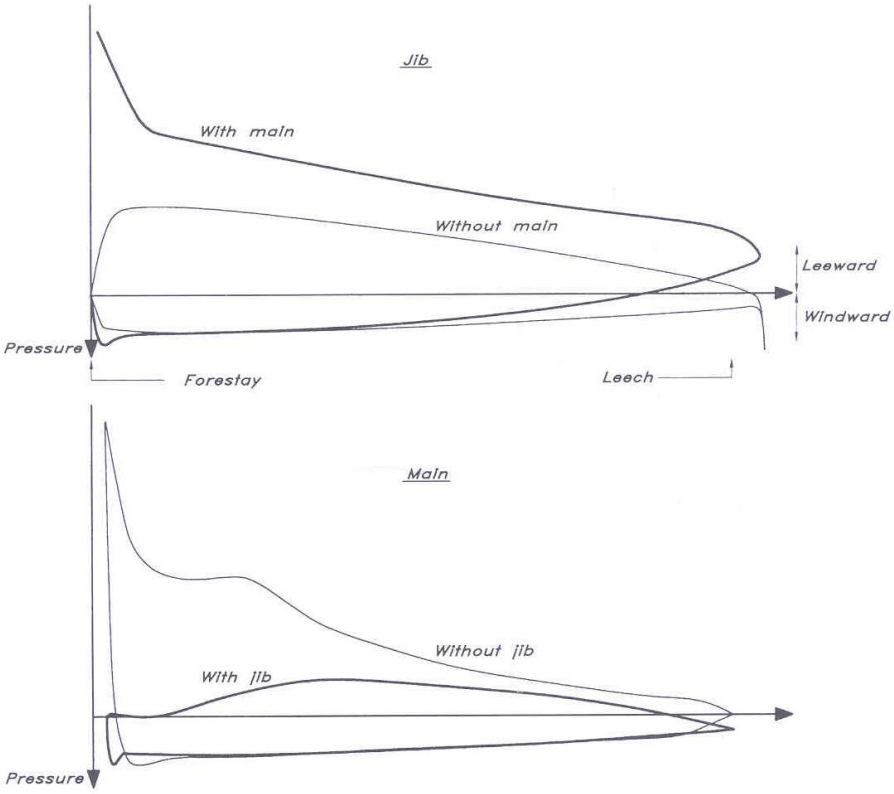

Figure 2.2

Circulation Theory of Lift

Another popular explanation for the creation of lift is the circulation theory. This theory was first suggested by Lancaster and further studies have been made by Kutta, Joukowski and Prandtl; all their work was well supported by experiments.

If the flow past a highly cambered asymmetrical aerofoil at zero angle of attack is considered, two fluid particles moving towards upper and lower surfaces of the foil section after negotiating the stagnation point S1 on figure 2.3-A travel along at equal speeds and since the upper surface is longer than the lower one the particle moving along the lower surface arrives to the trailing edge before the other. Naturally, its tendency is to go around the sharp turn at the trailing edge as seen on figure 2.3-B. At the initial stage of the flow, when the two mentioned particles meet somewhere on the upper surface near the trailing edge a second stagnation point forms, named S2. As the flow develops, due to viscosity of the fluid and strong inertia forces, this state of flow might not be maintained for long. The flow breaks away from the trailing edge forming the starting vortex seen in figure 2.3-C. [3]

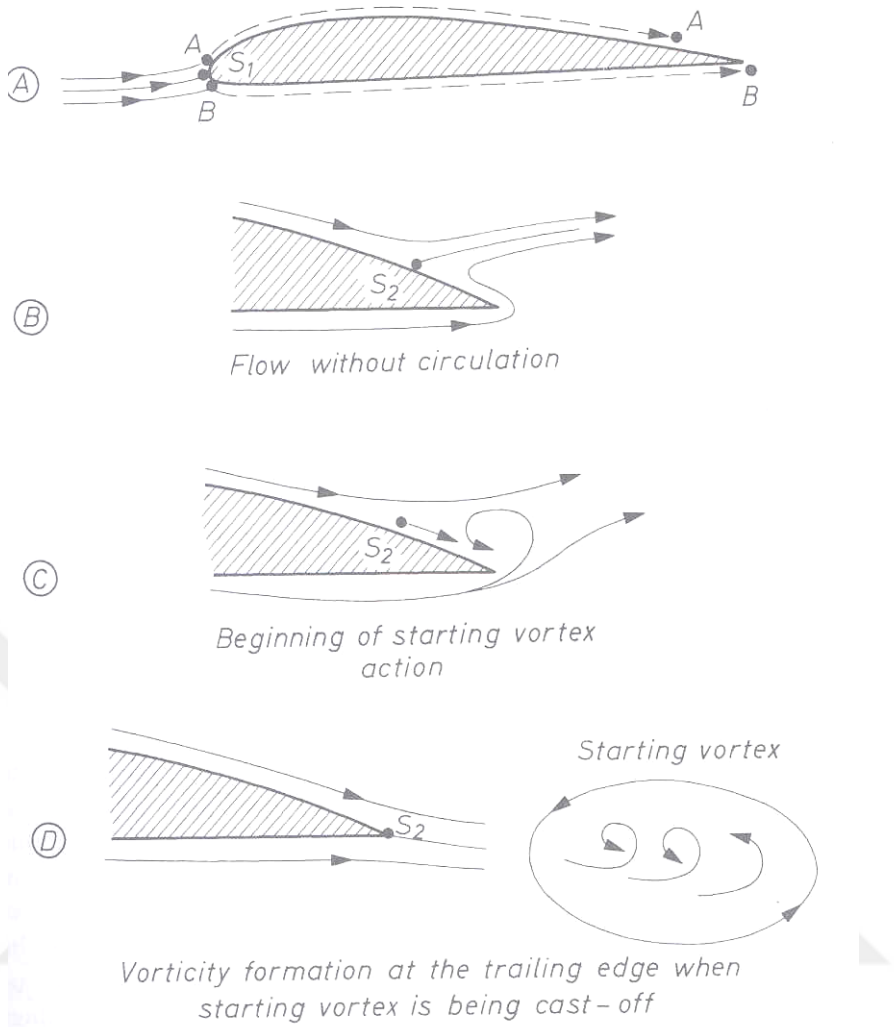

Figure 2.3

As the starting vortex rotates, due to Newton's third law of motion a counter rotation develops around the aerofoil in the opposite direction. This induced counter rotation appears as the circulation around the foil. Due to Newton's third law, angular momentum can not be created in a system without reaction. Quoting reference 1: "All forces arise from the mutual interaction of particles and in every such interaction the force exerted on the one particle by the second is equal and opposite to the force exerted by the second on the first".

Kutta and Joukowski have stated that as the starting vortex initiates the flow, it breaks away from the trailing edge and moves downstream in the wake. During this state, the stagnation point moves well aft, near the trailing edge in which case there is no difference between the velocities on the upper and lower surfaces while leaving the foil surface. In other words there is no physical implication that the starting vortex will be able to be maintained. The flow reaches a steady state after this point with a constant amount of circulation and hence lift force. The strength of the vortex that has been shed into the wake known as the trailing vortex

is dependent on the circulation around the foil. This leads to the fact that if the circulation around the foil is known, the lift force might be calculated.

Glauert has stated that due to the presence of negative and positive pressures on the faces of a foil, a spanwise flow will exist around the ends of the foil. The flow is redirected outwards on the pressure side and inwards on the suction side which induces a swirling motion at the trailing edge, dominantly on the tips of the foil. This swirling motion subsequently develops into the vortex sheet named as the trailing vortex which is shed into the wake. [3]

Munk has introduced the concept of "field of induced velocities" to aerodynamics, stating that the direction of the streamlines are altered ahead the foil and behind the trailing edge by the tip vortices giving rise to upwash and downwash. This concept will lead to definition of induced drag which will be discussed in 2.2.3. [3]

The horse-shoe vortex system consists of the starting vortex, the trailing vortices and the bound vortex which are all linked with each other due to Helmholtz Theorem which states that "a vortex once generated can not terminate in the fluid; it must end at a wall or form a closed loop". [6]

2.2.2 The Boundary Layer

The boundary layer around a body starts growing from zero thickness at the leading edge of the body and as the flow proceeds downstream shear stresses develop at the proximity of the surface due to large velocities in the mainstream and no-slip condition at the surface. This shear stress slows down the fluid particles which are close to the body. These relatively slow moving particles affect the latter ones and slow them down. As the fluid particles move downstream, this action of slowing down spreads further away from the body surface and the boundary layer of slowed down fluids increases its thickness. The usual convention about the thickness of the boundary layer is that it extends to the point where the velocity of that point is 99% of the free stream velocity in the normal direction to the body. [4]

Due to viscous effects present in the boundary layer, the forces acting on the body will mainly depend on the way that the boundary layer develops. Near the leading edge, the flow is likely to proceed in a smooth, ordered, streamlined fashion which is named to be laminar flow. As the fluid particles proceed along the surface, the flow develops into an irregular flow consisting of small scale eddies. In this region, the velocities are variable in magnitude and direction. This type of flow is named turbulent flow and it still follows the surface of the body. The change from laminar to turbulent flow is called transition. The pressure distribution influences the point of transition; a favourable pressure gradient (dropping pressure) delays the transition whereas an adverse pressure gradient (increasing pressure) nearly leads to an

immediate transition. In case the magnitude of the adverse pressure gradient is adequate enough, it might lead to a completely different case where the flow will not be able to maintain contact with the body surface; leading to separated flow. Near the leading edge, a high adverse pressure gradient is required to cause separation and a favourable pressure gradient can result in a reattachment of the flow. In this case, a leading edge separation bubble forms. [2]

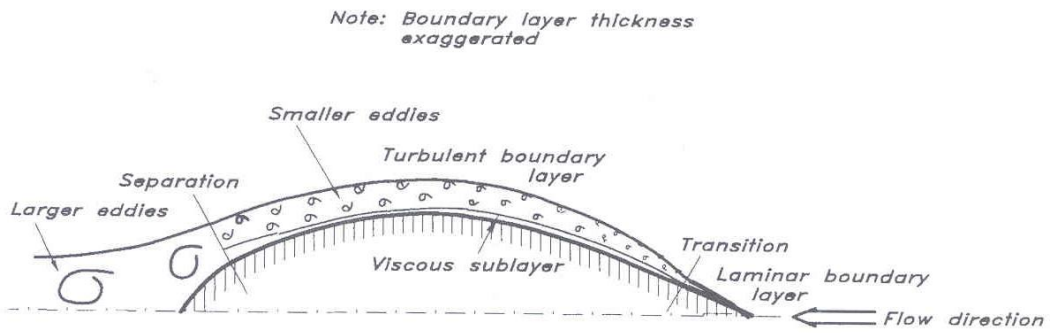

Figure 2.4

Figure 2.4 visualises the concept of laminar flow, transition, turbulent flow and separation as well as shows how large eddies form downstream of the body and form the wake region. [5]

2.2.3 Drag Breakdown of Sails

Figure 2.5 shows how to break the drag of the sails into components. This sketch does not include the windage drag caused by the existence of the rigging, superstructure and the non immersed portion of the hull. The profile drag consists of friction drag and pressure drag (viscous drag) which mainly depend on the Reynolds number and the geometry of the sails (camber, thickness, etc…). The remaining portion is the induced drag which is generated by the creation of lift. [3]

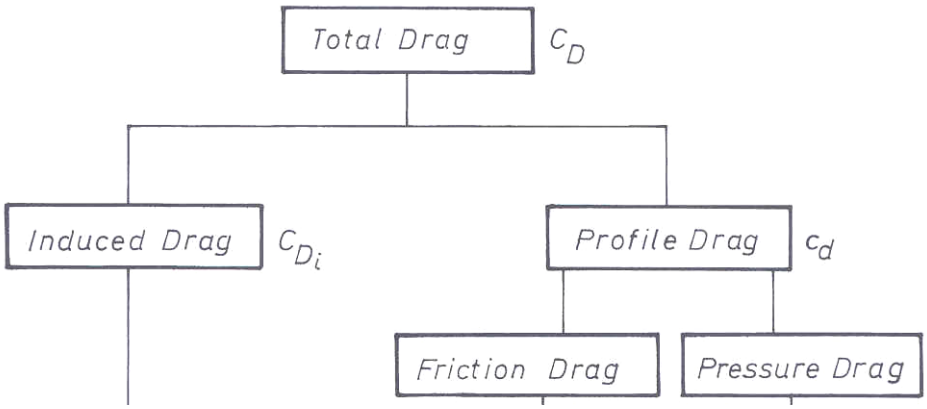

Figure 2.5

The induced drag depends on many factors; mainly the spanwise distribution of lift, aspect ratio, taper ratio and the amount of twist. In terms of lift distribution, an elliptical lift distribution leads to the least amount of induced drag. In order to achieve an elliptical lift distribution the sail shape does not necessarily has to be elliptic, since the loading depends on section shape as well as angle of attack and chordwise geometry. [3]

$$C_{Di} = C_L^2/(\prod \text{ x } AR_E)$$

The above equation is a representation of the induced drag; it varies with the square of lift and the inverse of aspect ratio. In order to identify the induced drag of sails, a useful way is to plot the drag coefficient versus the square of the lift coefficient as seen on figure 2.6. [3] Apart from the region of separated flow, this curve is linear and the slope of this plot is determines the aspect ratio which is fundamentally based on the effective rig height. Therefore, it can be stated that the most important parameter influencing the generation of induced drag is the effective rig height.

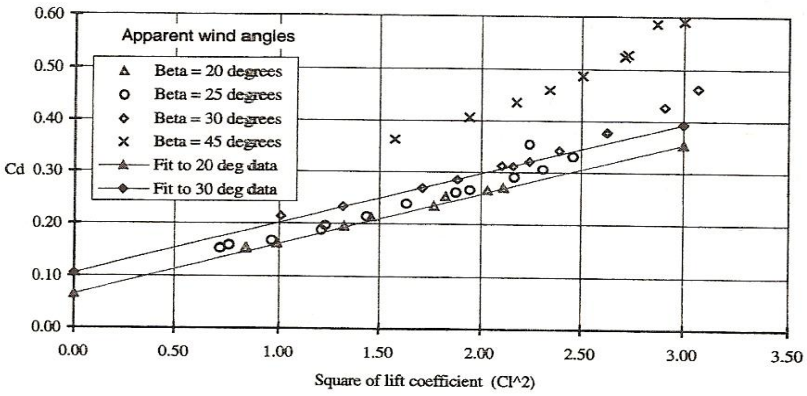

Figure 2.6

In order to have a quantifiable measure of the effective rig height, the influence of the water plane on the sails needs to be clarified. The mirror image method is used for this where the water plane is replaced by an inverted mirror image of the sails leading to the consideration of the problem of interaction of two sails. In reference 3 it is stated that “The flow pattern and interactions resulting from a combination of a real and a mirror image boat symmetrically placed on the other side of the boundary will be identical with the flow pattern on a real boat over a flat plane”. As a result, replacing the water boundary with an inverted sail leads to a better understanding and justification of the flow pattern around a single sail.

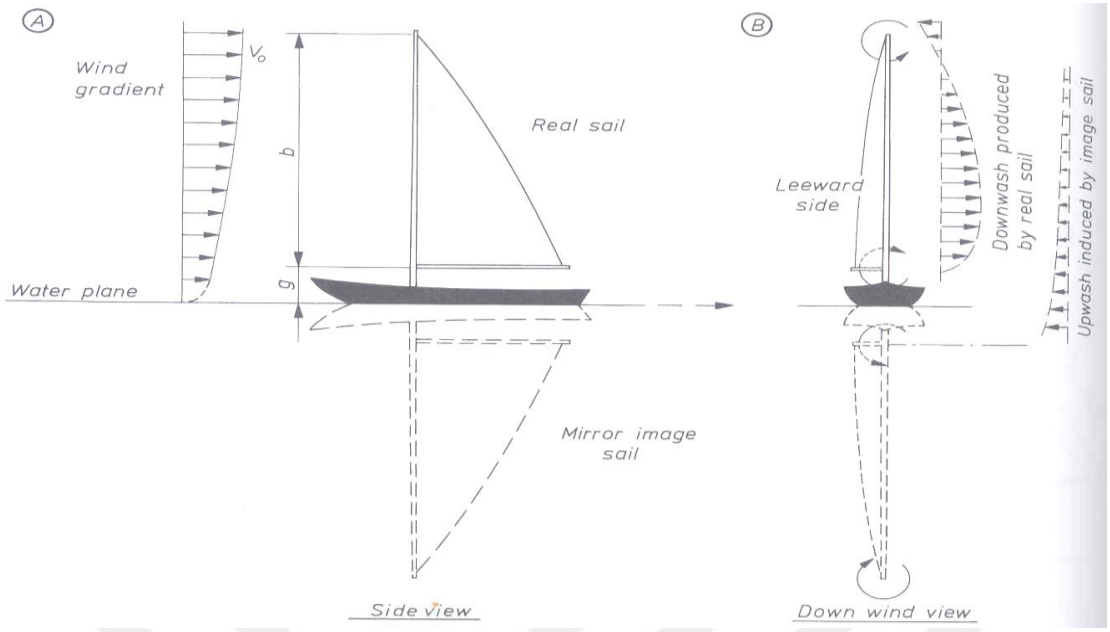

Figure 2.7

The above figure shows how the foils induce upwash outwards the tips and downwash between the tips. When two foils operate in close proximity, an upwash is induced by each foil on the other leading to a reduction in the downwash compared to the case of no interaction while the two foils are infinitely apart. Since the induced drag depends on the resultant downwash, the induced drag of the interacting sail will be less than the case of no interaction.

At this point, the definition of the proximity of the sails is of great value since the gap between the sails influence the interaction. Without the gap the effective rig height would be twice the rig height of the single sail, but since the gap is present the effective rig height will reduce to some value in between. This is hard to quantify in the absence of experimental data, but there exists practical methods. Hazen has suggested that the effective rig height might be taken as the 110% of the height from the top of the mast to the design water line while reaching and 110% of the height from the top of the mast to the deck edge while windward. [7]

2.3 Optimum Sailing Points

2.3.1 Upwind

The most important parameter in upwind sailing is the ratio of lift to drag. The lift to drag ratio can be expressed the drag angle which is the angle between the lift and the total force generated by the sails. A large drag angle implies a low lift/drag ratio.

The use of the drag angle for the aerodynamic and hydrodynamic forces leads to the derivation of the “Beta Theorem”. According to this theorem the angle between the apparent

wind and the course sailed is equal to the sum of the sail and hull drag angles. Naturally, both in aerodynamics and hydrodynamics maximum lift/drag ratios lead to a better upwind performance. [8]

2.3.2 Downwind

In downwind sailing, the aim is to produce the maximum drive force. On close reaching, the sails are mainly lift producing and it is the main contribution on the drive force. On broad reaching, both lift and mainly drag forces contribute to the total drive force. On the other hand, while running the sails are drag producing. [8]

3. WIND TUNNEL TESTING

3.1 Testing Procedure

Experimental Setup

The tests were conducted on a one metre yacht rig in the low speed section of 7' x 5' wind tunnel at the University of Southampton. The tunnel has a working section with dimensions of 4.6 metres and 3.7 metres and the model is accommodated on a turntable which also houses the six component dynamometer (see figure 3.1) that is designed by the Wolfson Unit. Forces and moments in three directions are measured on the yacht's body axis. It enables adjustment of headings in a range of 180 degrees which is measured by a potentiometer and monitored outside the tunnel.

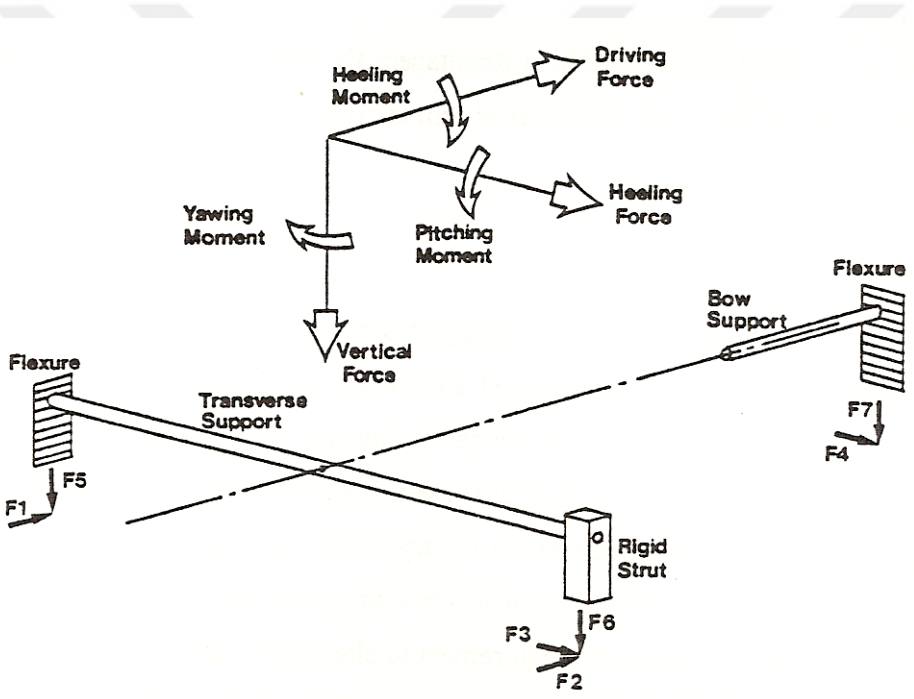

Figure3.1

Data Acquisition

Throughout the experiments, Wolfson Unit's software TurboAD was used for data acquisition. Once the desired speed is achieved, data is acquired over a fifteen seconds period. This is a need since the forces and moments measured are dynamic even the flow is uniform. During the fifteen second period, the forces and moments are acquired and the mean values are calculated and recorded subsequently. In order to minimise the magnitude of error, two acquisitions were made for each run consecutively and they were averaged. The stored data is then exported to Microsoft Excel as a spreadsheet.

In terms of data acquisition, two different approaches were used throughout the experiments. First of these is to adjust the sails in desired sheeting angles and twists prior to the run and to measure the forces. This is a systematic approach for getting the lift and drag coefficients for VPP input. This approach is logical in the sense that finding the equilibrium sailing points depends on both the aerodynamic and hydrodynamics forces and their equilibrium. The second approach is to run the tunnel in a desired speed and by remotely adjusting the sails to get the maximum drive force achieved. For this approach, the forces and moments are displayed in real time on the TurboAD screen, and by adjusting the sails, maximum drive force is tended to be achieved. This way is not suitable for upwind sailing conditions since at the condition of achieving maximum drive force, the heel force might be excessive for the hull to balance which would result in an undesirable condition. Also, the optimum sailing point might be somewhere where the drive force is a bit less than the maximum since increasing drive force does not necessarily mean that the speed of the boat is increased. Obviously, increased drive force results in increased heel force which is counteracted by the keel resulting in production of side force and hence induced drag. The induced drag produced by the keel and the hull by increased drive and heel forces might be excessive than the increased drive force which might result in the reduction of speed. The beta theorem presented in 2.3.1 explains this phenomenon in detail. However, obtaining the maximum drive force might be a useful method in downwind conditions and for comparison purposes such as the second and third sets of experiments made which are presented in section 3.4.

3.2 Scaling Methodology & Modelling Issues

The challenging task in wind tunnel experimentation is to simulate the real sailing environment as accurately as possible with minimising the assumptions and neglections. There are a few key aspects of the physics of sailing that need to be simulated in the wind tunnel to get accurate and reliable data. One of them is to simulate the real sea free surface boundary layer, which is achieved by placing the model on a trough filled with water. Also, the wind speed variation along the span and its twist needs to be simulated. However, this could not be achieved with the currently available equipment.

In case of testing models with scale factors, the flow regime is normally not identical to full scale due to being unable to achieve the full scale Reynolds numbers in the wind tunnel. It is well known that the sails experience forces which are highly viscous due to separation effects of the existence of the mast and operating close to stalling. Therefore, a Reynolds number based scaling needs to be applied, which leads to model speeds that can not be achieved with

the available facilities. As a result, without external means of increasing the so called effective Reynolds number, the forces experienced by the model and the full scale yacht will not be similar and therefore no Reynolds scaling might be applied. The way to overcome this problem is to use the smoothing screens at the inlet of the wind tunnel which are made of fine wire meshes that increase the effective Reynolds number by the order of six. [9]The chord length based model Reynolds numbers are generally below but close to $5x10^5$ which is the threshold of turbulent flow. Increasing the model Reynolds number by an order of six leads to a fully turbulent flow and therefore to a better modelling of leading and trailing edge separation points. Once the critical Reynolds number threshold and hence fully turbulent flow is achieved, the force similarity is achieved regardless of the difference of model and full scale Reynolds numbers.

Another aspect of wind tunnel experimentation is the consideration of the chosen speed. Care should be taken while assessing the speed relation between the model and the full scale yacht. Since no proper scaling law is being applied in order to eliminate the discrepancies between the loads on the sails due to the fact that the velocities required for scaling are too large for Reynolds scaling and too small for Froude scaling; the chosen speed must be avoiding structural problems with the rig and the flying sail shapes must be representative of the full scale yacht at the chosen speed.[9]

Quoting reference 9:"To perfectly model full scale wind speeds in the wind tunnel, much higher tunnel speeds and rigid sail models would be required. A rigid model can only simulate one trim setting at one apparent wind angle. Additionally, the "flying" shape of the sail would need to be known before building such a model. The GLMWT believes that the advantages of being able to evaluate infinitely trimmable models outweigh the model scale Reynolds number discrepancy."

In order to get reliable data for full scale predictions, the raw data should be analysed with suitable scaling methodologies. There are several ways to scale raw wind tunnel data. Unfortunately, not much published work that deal with model-full scale performance comparison exists. Some experimenters use the lift and drag coefficients without applying any corrections. Others apply a maximum achievable lift coefficient correction since at high Reynolds numbers the maximum achievable lift coefficient might be different due to the different flow regime resulting from increased Reynolds number. This is in fact hard to predict since the behaviour is different for different foil types and there are not any published work that shows a quantifiable measure of the correction to be applied for sails. [11] Some scientists apply a method which is analogous to ship drag scaling where the friction drag is

recalculated with the increased Reynolds number and the rest of the drag is scaled with the dynamic pressure and planform area. [12]

3.3 Initial Setup

Dynamometer Calibration

Initially, the dynamometer needs to be checked by calibration to ensure that the forces and moments measured are accurate. This is done by placing calibration weights of known values on rods that are attached to the dynamometer system with the aid of pulleys and measuring the forces and moments on the acquisition software.

Model Positioning & Control

Once the system is calibrated, the model is positioned on the turntable and the remote control of the winches is connected. There are two winches on the model which control the sheeting angles of the main and the jib via a pulley system as seen in figure 3.2. The remote control is situated outside the tunnel and real time adjustments can be made to maximise the drive force obtained. This is beneficial in terms of the accuracy since adjustments made while a person is inside are influenced by the alteration of the flow due to the considerable blockage effect of a person inside the tunnel.

Figure 3.2

The housing system for the model on figure 3.3 consists of three bars, one placed at the bow, the other two at each side that are connected to the force blocks. With suitable arrangements, the model can be heeled to a constant angle but the model used did not have the mentioned arrangement, all tests were carried out at upright form. This is acceptable in the sense that VPP programs apply a correction for the upright lift and drag coefficients while converting them to heeled lift and drag coefficients.

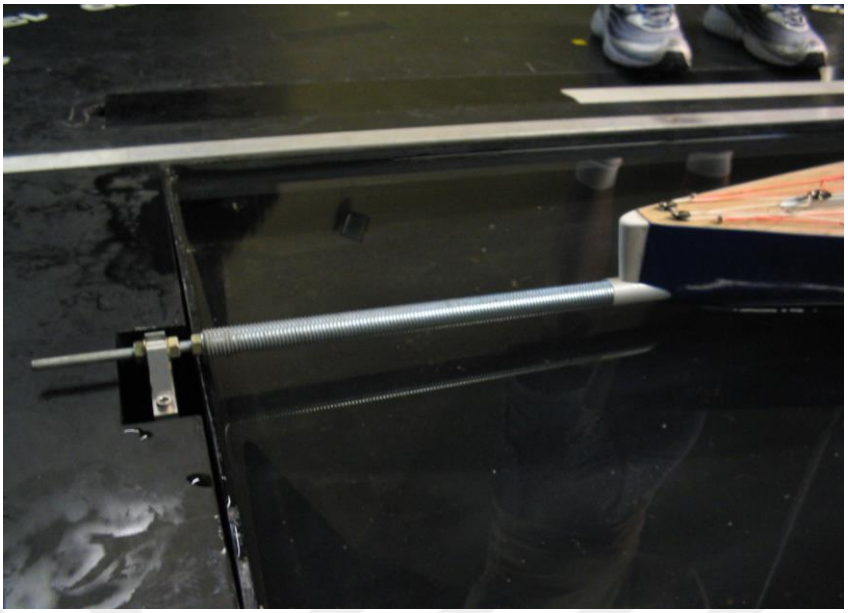

Figure 3.3

3.4 Different Configurations Tested

Three sets of experiments were made for different purposes. First of these was aiming to obtain a systematic measure of lift and drag coefficients in close hauled sailing conditions for a range of twist and sheeting angles for two different speeds which were 5 m/s and 9 m/s. The sheeting positions were measured from the centre line in millimetres. Twist was measured as the distance from the centre line to the half height trailing edges of the sails. The force values obtained would then be used in VPP input of lift and drag coefficients for performance prediction later on. The heading angle was fixed at 30 degrees and main and jib sheeting and twist angles were varied systematically to see the trends and to comment on the effects of these variations.

The test matrix for these set of experiments is presented on table 3.1.

sheeting combination	jib sheeting (mm)	main sheeting (mm)	jib twist (mm)	main twist (mm)
1	50	10	30	50
2	50	10	30	70
3	50	10	50	50
4	50	10	50	70
5	50	40	30	50
6	50	40	30	70
7	50	40	30	50
8	50	40	50	50

9	50	40	50	70
10	75	10	30	50
11	75	10	30	70
12	75	40	30	50
13	75	40	30	70
14	75	40	50	50
15	75	40	50	50
16	75	40	50	70

Table3.1

The purpose of the next set of experiments was to assess the effect of deck fairing on lift and drag values. Headings between 30 and 180 degrees were tested as seen on the test matrix in table 3.2 for a constant speed without any deck fairing. The tests were repeated with the foredeck faired (figure 3.4) and with both the fore and aft decks faired subsequently to see the influences on the lift and drag forces. The sails were sheeted independently to maximise drive force and the resulting sheeting angles were recorded.

heading degrees	without fairing	fore deck faired	fore & aft deck faired
30	5 m/s	5 m/s	5 m/s
40	5 m/s	5 m/s	5 m/s
50	5 m/s	5 m/s	5 m/s
60	5 m/s	5 m/s	5 m/s
90	5 m/s	5 m/s	5 m/s
135	5 m/s	5 m/s	5 m/s
180	5 m/s	5 m/s	5 m/s

Table3.2

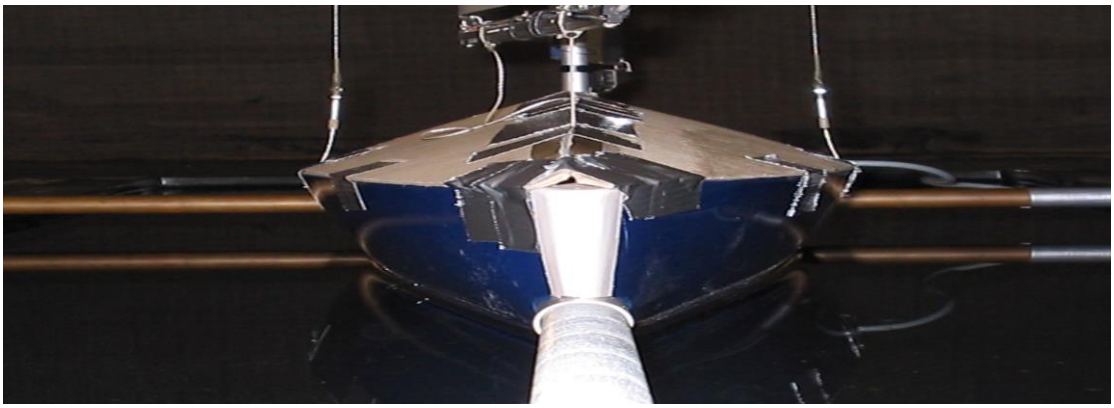

Figure 3.4

The last set of experiments was based on obtaining a set of lift and drag coefficients for VPP input in running conditions without the spinnaker. Currently available VPP programs have force models which by default assume that a spinnaker is present on the yacht. Therefore, a set of experiments were made with the main and the jib only, to obtain the lift and drag coefficient for this sail suite.

There are two ways of sail setting in running conditions which are running goose winged where the main and the jib are on different gybes and running fully sheeted out where the

main and the jib are on the same gybe. While obtaining the lift and drag coefficients for VPP input, comparisons will be made between these two settings. A range of headings between 120 and 180 degrees were tested with an increment of 10 degrees for a speed of 4 metres per second with the two different settings. The test matrix for these experiments might be found on table 3.3.

Also, for the sake of drag breakdown, windage of the hull and the rig as a whole and windage of the hull without the rig were measured for headings between 0 and 180 degrees with an increment of 30 degrees.

heading degrees	running on the same gybe	running goosewinged
90	6.5 m/s	6.5 m/s
130	6.5 m/s	6.5 m/s
140	6.5 m/s	6.5 m/s
150	6.5 m/s	6.5 m/s
160	6.5 m/s	6.5 m/s
170	6.5 m/s	6.5 m/s
180	6.5 m/s	6.5 m/s
190	6.5 m/s	6.5 m/s
200	6.5 m/s	6.5 m/s

Table 3.3

For CFD validation, it was anticipated to conduct a different set of experiments as it was decided to restrict the validation process to upwind conditions. Since a large portion of the testing includes downwind conditions and the upwind conditions tested were so plenty in number to include in CFD validation scheme, a set of experiments were made with sail suite 1, on a speed of 3.5 metres per second, between heading angles of 30 and 90 degrees, with an increment of 10 degrees. Maximum drive forces were achieved by adjusting the sails real time and the data were acquired. Once the data was acquired for each experiment, the wind was run once more with a person inside the tunnel whose task was to take aerial pictures to use as an input for CFD calculations.

3.5 Interpretation of Raw Wind Tunnel Data

3.5.1 Boundary Corrections

It is essential for the raw data obtained from the wind tunnel measurements to be corrected in the appropriate fashion so that the magnitude of error in the measurements are minimised as much as possible and they are more representative of the actual sailing conditions experienced in real time. Obviously, the flow regime in a wind tunnel can not fully represent the actual environment being simulated due to several reasons. These reasons are identified and the ways to take them into account are presented in this section.

Solid Blockage

In real operating conditions for sailing yachts, the planform area of the sail set is infinitely smaller than the sectional area of the air domain. However, in wind tunnels the ration of the area of the sail set to tunnel cross sectional area is typically 5% with a variation between 1-10%. This leads to the blockage of the model that is accommodated in the tunnel influencing the oncoming flow resulting in variations in the dynamic head of the flow. The area through which the air flows is reduced and hence due to continuity and Bernoulli's equation the velocity of the air is increased. For the experiments made this ratio was 2.3% for sail suite 2 and 3.3% for sail suite 1. First order values of the area ratio are assumed to be less influential on the results and therefore a correction is not necessary. [11]

Wake Blockage

The wake blockage is a consequence of a finite body wake which has a similar effect with solid blocking. The ratio of wake area to tunnel area is the key parameter which is in fact hard to quantify. Increasing wake size results in an increase of measured drag that should be corrected for. Maskell has suggested a wake blockage correction ratio which was then modified by Cowdrey. [7]

$$C_{Dc} / C_{Du}=1\text{-}m \times (S / C)$$

Streamline Curvature

In a closed wind tunnel, the variation in the streamline curvature of the flow around a body compared to an infinite domain leads to an increased angle of attack, lift and moments. The correction method for this effect is as follows. [11]

$$\sigma = (\Pi^2 / 48) \times (c / h)^2$$

$$\Delta C_L=\sigma \times C_L$$

$$\Delta\alpha=\delta \times (S/C) \times C_L$$

$$\Delta C_{Di}=\delta \times (S/C) \times C_L^2$$

This alteration to the flow is significant only for upwind conditions and therefore it might be neglected for downwind cases.

3.5.2 Wind Speed Correction

The wind speed in the tunnel is measured via a pitot tube which is situated in the high speed section of the tunnel. The reading is in the units of mm of water. The static head in the pitot tube is equal to the dynamic pressure of the air and Bernoulli's equation is used to convert the static head to the velocity of air in metres per second: [11]

$$V_{air} = \sqrt{2 \times g \times h \times (\rho water - \rho air) / \rho air}$$

Since the speeds are recorded in terms of the static head values, a correction must be made due to varying temperature in the test section. The test section is heating up gradually as the flow speed was being increased due to the increased energy in the flow. Also, after every run for resetting the model and acquiring a zero run, a certain time needs to be spent while the temperature drops. This variation, combined with the fluctuations in the atmospheric pressure, even being small, changes the velocity magnitude in the test section and it was taken into account by the calculation of the density of air at that temperature and pressure.

ρ_{air}=Air Pressure (Pa)/ [287.05 x Temperature of Tunnel (K)]

Theoretically, the next step in terms of speed correction would be the solid blockage correction due to flow being accelerated. However, as mentioned the solid blockage effect is negligible due the relatively small dimensions of the yacht model being tested.

The algorithm for corrections starts with the temperature and pressure correction for velocity. Then, the zero values before and after each run are averaged and filtered out from the forces and moments. This is done since the dynamometer is being pushed in one direction for a long time and there might be a measurable residual force on the dynamometer which needs to be filtered out. Also, changing the settings or the heading angle has pretty much the same effect. The scheme of taking zeroes before and after the runs and averaging those increases the accuracy of the results compared to taking zeroes only before each run since the zero point moves from the first zero to the second during each run. Therefore, the zero point during the run is somewhere between the two and also the variation is known to be linear from calibration which mean that averaging the zero values is the best approximation.

3.5.3 Viscosity Correction

The variation of dynamic viscosity with temperature was accounted for during interpretation of the data. This effect combined with the variation in density leads to a change in Reynolds number which is used to calculate the skin friction coefficient. [12] The variation of dynamic viscosity with temperature might be seen on figure 3.6.

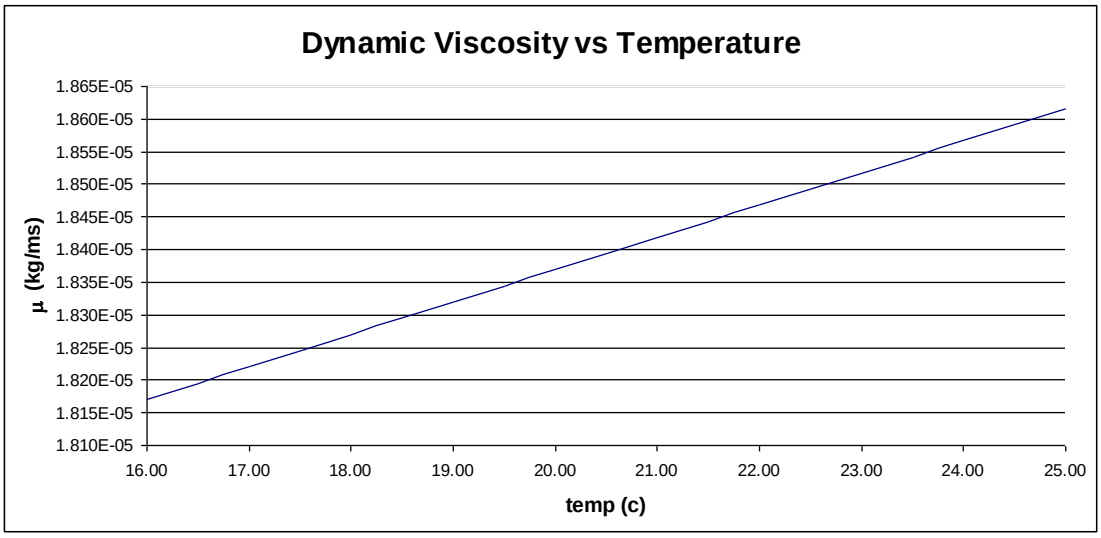

Figure 3.6

3.5.4 Transformation of the Forces into Lift and Drag

The measured forces in the wind tunnel were in model body axis, namely drive force and heel force. These forces need to be resolved in the wind axis in order to obtain the lift and drag force of the sails for further analysis. The formula used for this transformation is as follows:

$$L = D_F \sin\beta + H_F \cos\beta$$
$$D = H_F \sin\beta - D_F \cos\beta$$

For convenience, the forces were converted to non dimensional coefficient form by dividing with the planform area of the sails and the dynamic pressure head.

3.5.5 Drag Breakdown

Section 2.3.2 explains the drag breakdown of sailing yacht rigs in detail. The important point to mention at this stage is the calculation of induced drag. Since there was not a measure of effective rig height for the particular rig, and suitable experiments were not made to be able to plot C_L^2 versus C_D to see the trend and hence calculate the induced drag and the effective rig height; reasonable assumptions needed to be made. Hazen's suggestion was a good starting point at this phase. Hazen suggests that the effective rig height might be taken as the 110% of the height from the top of the mast to the design water line while reaching and 110% of the height from the top of the mast to the deck edge while windward. This reduction is due to the loss of endplate effects once the jib is raised off the deck while windward. [7] In the case of the one metre yacht rig, there is always a gap between the sails and the deck present, therefore it was supposed to measure the distance from the deck at all conditions. For both windward and reaching conditions the value for the effective rig height was assumed to be 110% of the distance from the top of the mast to the deck edge.

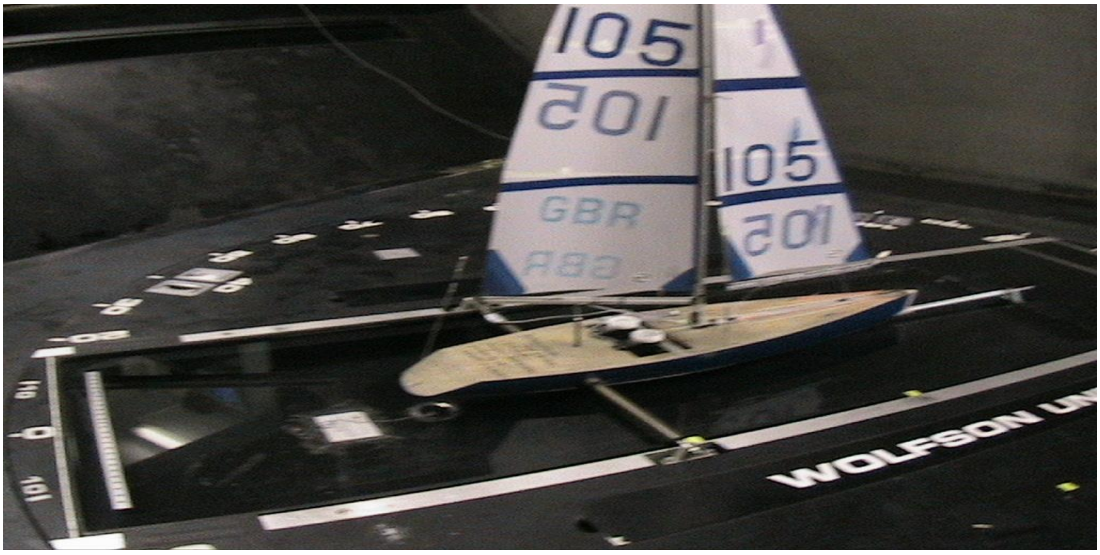

Figure 3.7

The above figure show the gap that causes the loss of endplate effects resulting in as reduction of effective rig height whereas figure 3.8 shows an America's Cup yacht where the sails are sheeted in such a way that the foot of the sails are in close proximity with the deck edge that increases the effective rig height of the yacht.

Figure 3.8

This assumption seemed to have worked pretty well, since the trends in the data show that in upwind sailing conditions, there is little viscous drag due to separation at realistic sailing conditions and in downwind conditions the majority of the drag is due to separation and hence viscous and there is an insignificant induced drag. Obviously, sails operate at low angles of attack in upwind where there is not a significant amount of separation. This was observed in the drag breakdown from the values of viscous drag. As the sails are over sheeted in upwind, with increasing angle of attack the viscous drag due to separation tends to increase. This also was observed from the tell tails during the experiments where over sheeted sails tended to reach stall.

3.5.6 Correction Algorithm for the Raw Data

The lift and drag forces obtained were non-dimensionalised for applying the suitable corrections. First of all, lift force was corrected for the stream line curvature effect. Afterwards, the drag force was corrected for the wake blockage. The next step was to break the drag down in the appropriate manner as mentioned in section 3.5.5 so that the induced drag can be corrected for streamline curvature. Once the corrected induced drag is added to the rest of the drag which consists of frictional, viscous and windage drag; the overall corrected drag value is obtained. With these corrected values the lift to drag ratio was calculated. Afterwards, the heading values were corrected for streamline curvature. Once the lift and drag forces, velocities, headings are corrected; their corrected values were used to obtain the corrected drive force and heel force.

4. PRESENTATION OF WIND TUNNEL TEST RESULTS

4.1 Wind Tunnel Test Results

The raw data for the whole set of experiments might be found in appendix I. In this section, only the comments on the results and possible reasons for errors will be presented. Also, please note that the experiments that were done for CFD comparison will only be presented in section 6.

Variation of Lift and Drag Coefficients with Changing Sheeting and Twist angles in Upwind Conditions:

As it might be seen from the test matrix on table 3.1, the model was tested with the mentioned sail settings at two different speeds. When the forces obtained from these experiments are non dimensionalised to coefficient form by dividing with the density, area and the square of speed,

they become independent of geometry and speed and hence it is not expectable to detect a difference in the coefficients with increasing speed. However, this was not the case in the experiments made. This was highly predicted during experimentation, and the exact reasoning behind this problem was known. During the experiments, the pre determined sail settings were made with a speed of 2 metres per second prior to each run with a person inside the tunnel manually since it involves the adjustment of twist which can only be done manually. This was thought to be of convenience for all the experiments of this set. Unfortunately, the setting made at 2 metres per second could not be maintained at the actual test speeds which were higher than it. This was due to the increased loads on the rig being excessive for the standard pulley winch arrangement to withstand. The sheeting and twist set prior to the runs were actually increasing during the runs and the increase was different for each particular speed which leads to the variation of the force coefficients.

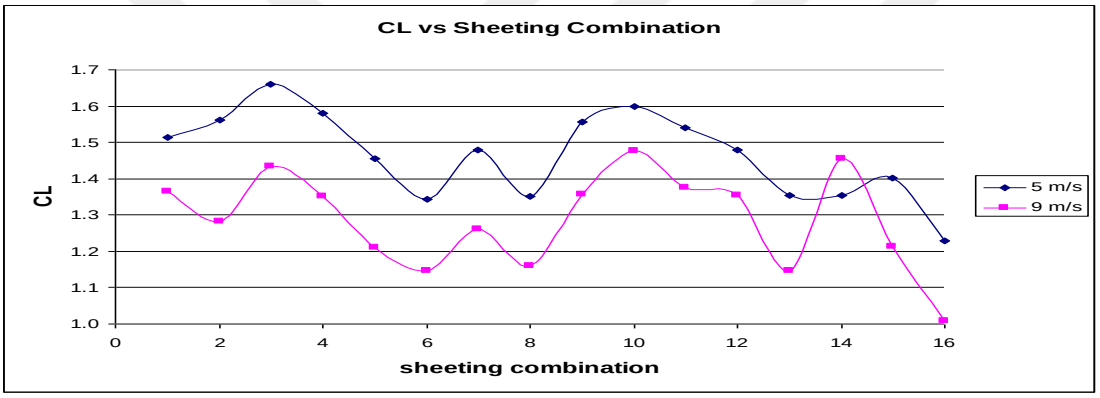

Figure 4.1

Even it is known that there is a degree of error in the results, similar trends were observed on the results for the two different speeds as it might be seen on figure 4.1 which means that there is a certain amount of reliability in the results in order to make analysis. For convenience, the sheeting and twist values were said to be representative of initial settings at a speed of 2 metres per second and the resultant sheeting and twist values are not going to be regarded neither for the analysis nor the VPP input to be done later on.

For upwind sailing, the most important parameter to be maximised is the lift to drag ratio. This phenomenon was presented in the Beta Theorem at section 2.3.1. As said before, similar trends were observed for the two different speeds and useful information was gained from the experiments. Figure 4.2 shows the lift to drag ratios for different sail setting.

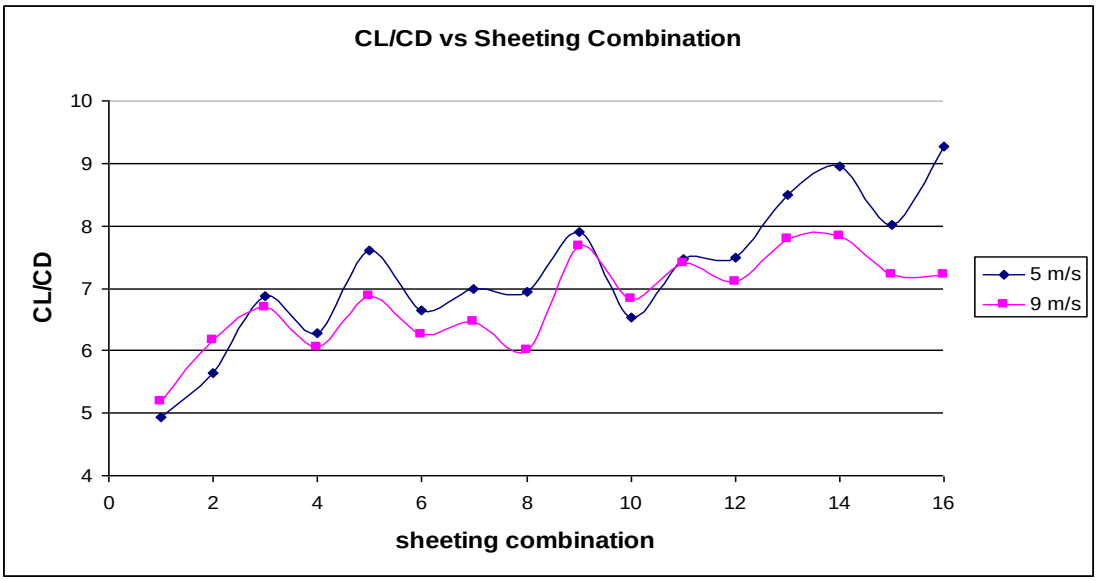

Figure 4.2

The above graph makes more sense if it is compared to the graph of drive force. When figure 4.2 and figure 4.3 are compared, it is seen that the sail setting which gives the maximum drive force is not necessarily the best sailing condition since the maximum lift to drag ratios obtained do not comprise of the sail settings which result in maximum drive forces. The implementation of the beta theorem has proven to be very useful in the understanding of the upwind sailing phenomenon, and the results obtain are approving the facts underpinned by the theorem.

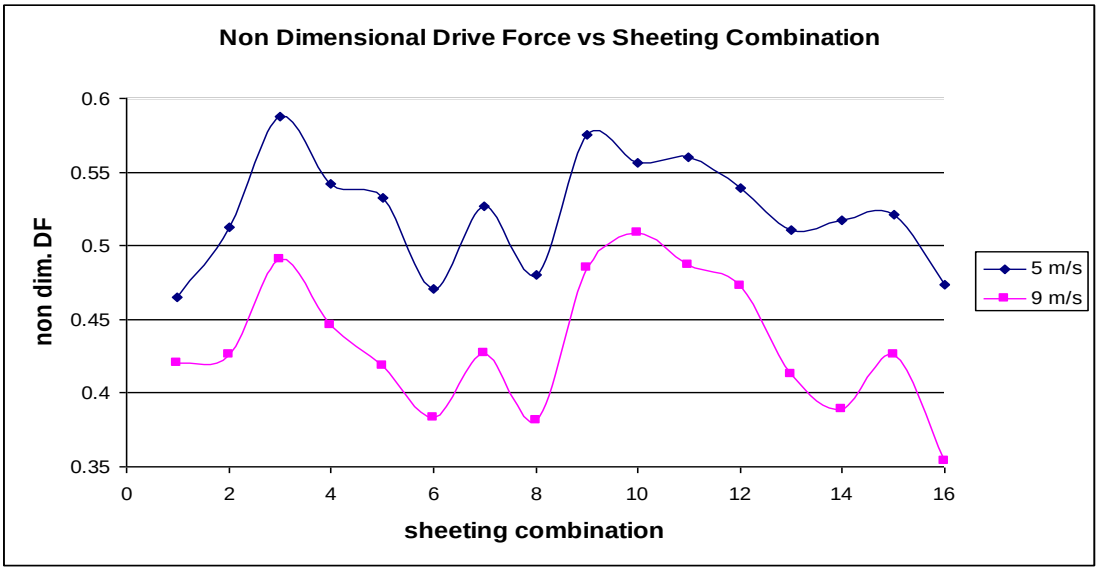

Figure 4.3

Effect of Aerodynamic Deck Fairing on the Performance of the Yacht:

Previously, it was anticipated that the deck equipment on the one metre class yachts was affecting the overall performance of the yacht. In order to assess the possibility of enhancing

the performance, the deck was covered with a fairing and the changes in the maximum drive forces obtained were compared.

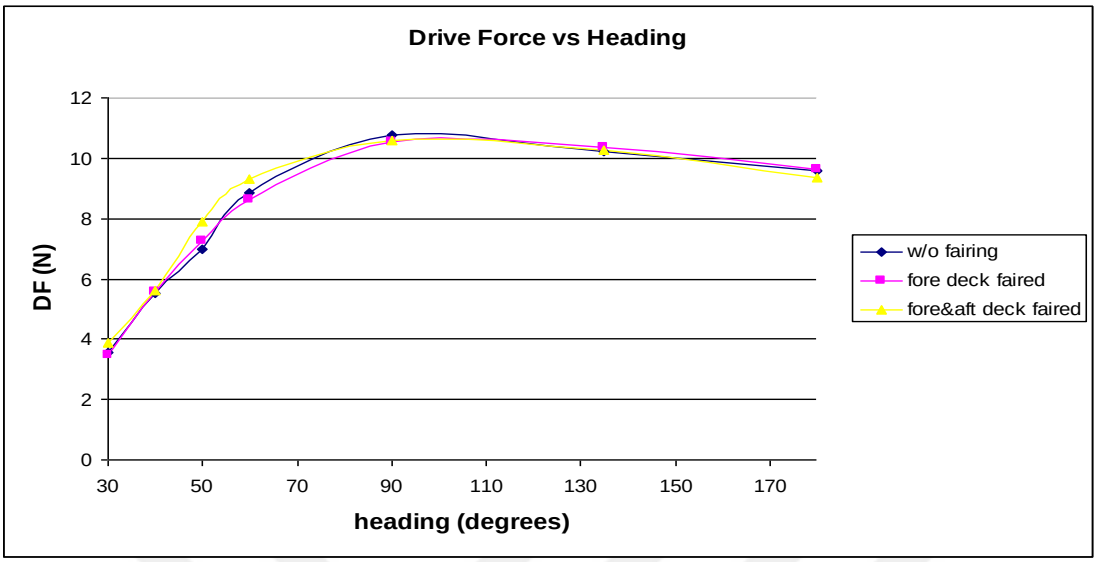

Figure 4.4

The above plot shows that there was not an overall significant gain in drive force with the deck fairing. However, there is gain in upwind, but the penalty is paid in downwind where there is a slight loss in drive force. Figure 4.5 shows that the lift to drag ratios are improved when both the fore and aft decks are faired which is a sign of better upwind performance.

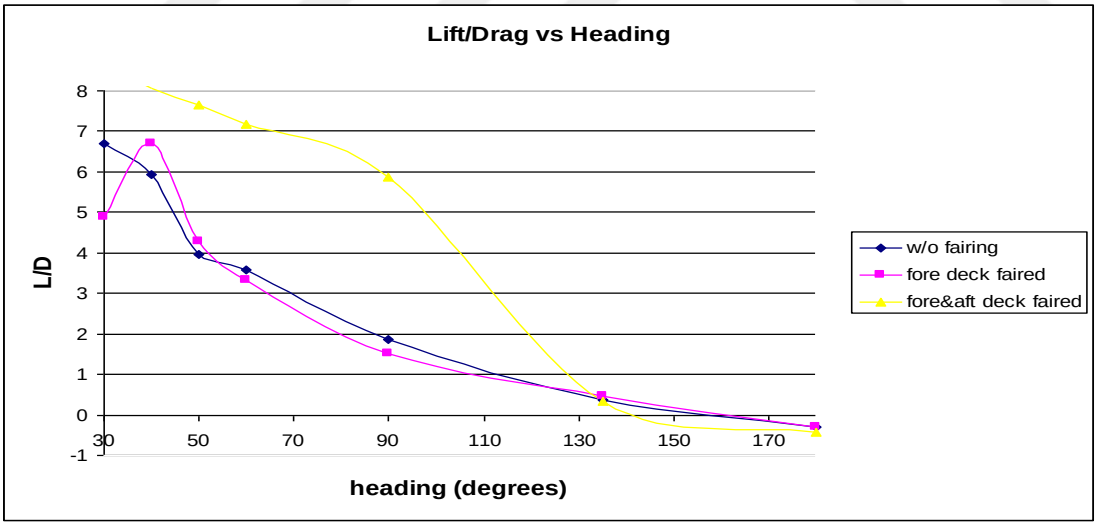

Figure 4.5

Even the plots of drive force and lift to drag ratio show signs of a slight increase in performance in upwind, it would be beneficial to analyse the problem in a VPP to see the actual differences in the speeds obtained before making a decision of fairing the deck.

Comparison between Running on the Same Gybe and Running Goosewinged:

The results of these experiments were highly predictable in the favour of running goosewinged in view of the fact that running on the same gybe is not a usual practice in sailing since the main with a relatively bigger area is screening the jib which is preventing the jib from acting as a parachute. This results in production of less drag and therefore less drive force in running conditions. Figure 4.6 shows the differences in the maximum drive forces obtained in both cases. As seen, there is a significant raise in the drive forces on the goosewinged condition.

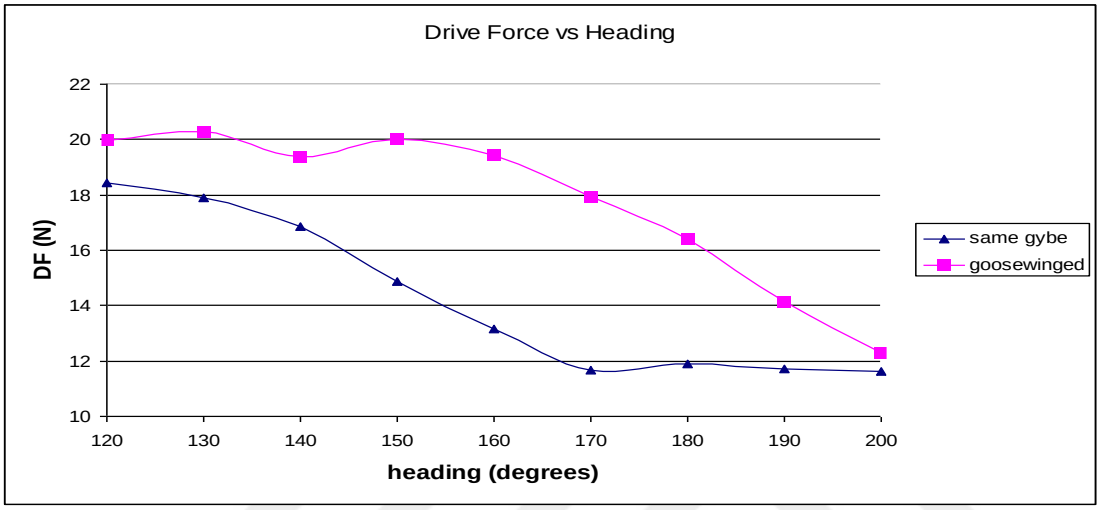

Figure 4.6

4.2 Possible Reasons for Errors

Apart from the errors related with the methodology of experimentation mentioned previously, there were other probable sources of errors that might have affected the results.. Even there is not a quantifiable proof that these errors have influenced the results, it is possible to estimate the sources for this type of errors within reasonable postulation.

One possible source of error is the dynamometer itself. Even the error is tried to be minimised by acquiring data without any load to “zero” the system before and after each run, there is a certain degree of uncertainty in the accuracy of the system. A reasonable estimate for this type of error is about 0.1 N.

Another possibility of error is the adjustment of the heading angle. This is controlled manually and it is measured by a potentiometer and the heading angle is monitored outside the wind tunnel on a digital panel. There were slight deviations between the desired and actually adjusted headings at some cases which was quantifiable. The deviation in the heading angle was maximum 0.2 degrees in the worst case. This amount of change can be considered as small and therefore it can be concluded that it would not influence the results dramatically.

The measurement of the static water head for the velocity might be a possible source for error. This was monitored on an analogue gauge outside the tunnel. The possible deviation from the desired water head might be about 0.1 millimetres which is relatively slight and hence it can be considered as trivial.

It is worth noting that the measurements were made only on port tack and this might be a cause of error. This way of testing does not take into account the imbalances that might be present on the model. The most optimal method to eliminate this sort of inaccuracy would be to test at both tacks and average the results.

5. CFD CALCULATIONS

5.1 Introduction

In order to validate the experimental results, it was decided to carry out CFD calculations. Compared with the rest of the computational methods -mainly with surface panel methods-, RANS solvers have got numerous advantages in resolving the salient features of viscous flows. This enables the chance of capturing the flow details in a more realistic way where the effects of viscosity can be simulated. At the same time there is a trade of between better accuracy and increased computational effort. However, due to its better accuracy and confidence gained from the industry, it was decided to use the RANS code Fluent and its pre processor GAMBIT for all the simulations made.

It is well known that the physical phenomenon and mathematical modelling behind the RANS solvers are very well tested and it is a useful tool that can be incorporated both into the design and research about yachts. However, in terms of sail performance prediction, limited amount of work has been done as yet and the aim is to find ways to achieve a realistic solution within reasonable accuracy. Therefore, it was deemed necessary to assess the capability of the Fluent code in terms of sail performance prediction first of all. This assessment consists of achieving a convention on all the user based parameters that influence the solution of the sail performance problem.

Inaccuracies and uncertainties that might be associated to a CFD solution mainly depend on the user's manipulation on the adjustable parameters within the code. Therefore, it is the best practice out of all to start with a two dimensional simplified case of the exact problem and try to see the influence of the user based parameters on the solution. In order to ensure that all the user based parameters are optimised for the sail performance prediction problem and that there will be a high level of confidence in the CFD results obtained, it was decided to adopt a systematic approach to tackle the problem during the setup process. All the user based parameters were investigated in detail to find the ones that best suit the particular problem.

5.2 The Setup Process

5.2.1 Turbulence Models and Wall Treatment

In this section, wall treatment and the turbulence models available in Fluent will be summarised and their suitability for the particular problem will be assessed.

General Terminology of Wall Treatment

The most important parameter about the wall treatment process is the wall distance unit, named Y+. It is equal to the distance from the wall multiplied by the ratios of frictional velocity and free stream velocity. Y+ is the main control that the user has over wall treatment. Different turbulence models demand different y+ values for the first cell attached to a wall since different turbulence models are valid down to different regions of the boundary layer owing to the different assumptions associated with them.

Spalart - Allmaras Model

This one equation model was initially developed for unstructured codes for use in the aerospace industry. It is also suitable for use with structured meshes. It is economical and accurate for wall bounded flows and flows with mild separation and recirculation. On the other hand, it has weaknesses in massively separated flows, free shear flows and simple decaying turbulence. It was originally intended to be integrated through the log layer but Fluent's implementation can also use law of the wall. Therefore, it can be used for both coarse and fine meshes and no specific wall treatment is necessary for this model. [14]

Standard k-ε Model

It is a high Reynolds number model which is robust, economical and it has reasonable accuracy for a wide range of flows. It has weaknesses such as flows involving streamline curvature, swirl, rotation, separation and low Reynolds number. Even it is highly popular in the industry, it should be handled with precaution and its suitability for the particular problem has to be assessed carefully.

In order to eliminate the deficiencies of the standard k-ε model, its variants have been developed. [14]

RNG k-ε Model

This model has an enhanced performance in strained flows and streamline curvatured flows. However, it suffers from bad convergence; more iterations might be required to obtain convergence. Also, it has still not gained confidence in the industry yet. [14]

Realizable k-ε Model

It has been performing better in complex flows with large strain rates, in the case of recirculation, rotation, separation and strong pressure gradients. It also has better convergence compared to the RNG model. [14]

Wall Treatment for k-ε Models

All the k-ε models are valid in the turbulent core region and through the log layer. Therefore, special wall treatment is necessary since the equations can not be integrated down to the wall. For high Reynolds number flows and flows without complex near wall phenomenon such as strong body forces, severe pressure gradients, rapidly changing fluid properties; standard wall functions might be used where the boundary layer shouldn't be resolved down to the wall. For adverse pressure gradients and separation effects, non equilibrium wall functions are more suitable. If there is still an uncertainty that using wall functions is not appropriate, the boundary layer might totally be resolved and the option of enhanced wall treatment might be used. This results in an excessive computational effort since the number of cells required to resolve the boundary layer are too high compared to using wall functions. [14]

Standard k-ϖ Model

This model is a popular alternative for all the k-ε models. It has a weakness of strong sensitivity to inlet turbulence specifications. Also, the mesh needs to be resolved down to the wall. Therefore, coarse meshes can not be used with this model. It can take into account transition effects optionally. [14]

SST k-ϖ Model

This model was developed to be used for flows that can not be accurately predicted with the available k-ε and k-ϖ models. These mainly consist of boundary layer flows under severe adverse pressure gradients and separated flows. This model is the most suitable for massively separated flows; however it suffers from poor convergence at some cases. [14]

Wall Treatment for k-ϖ Models

The only option of wall treatment for k-ϖ models is the enhanced wall treatment. Therefore, the boundary layer should be resolved down to the wall. [14]

Reynolds Stresses Model

This model is based on solution of the exact transport equations for the Reynolds stresses. Therefore six equations are solved in a three dimensional flow problem. This ends up roughly in a 50% more CPU time and 20% additional memory requirement. Also, the strong coupling between Reynolds stresses and the mean flow results in excessive number of iterations for

obtaining convergence. However, it has superior performance in flows involving streamline curvature, swirl and rotation. [14]

Wall Treatment for Reynolds Stresses Model

The wall treatment for Reynolds stresses model is analogous to k-ε models where a decision has to be made about the way of resolving the boundary layer. [14]

General Guidelines for Turbulence Modelling and Wall Treatment

It is a known fact that there is no universally valid turbulence model that gives accurate results for all diverse types of flows. As a result of this, the effect of using different turbulence and the sensitivity of the results on this variation should be assessed. If wall functions are being used, the grid should be arranged so that the Y+ values are in the appropriate range specified by the software vendor. Also, it is recommended to avoid triangular or tetrahedral elements on boundary layer grids.[15]

5.2.2 Solver Settings

There are two solver options in Fluent; the segregated solver and the coupled solver. The decision of the solver scheme mainly depends on the presence of compressibility effects in the flow. Since there aren't any compressibility effects in the sail performance prediction problem, the segregated solver was the suitable one which is intended for incompressible flows.

The discretisation schemes also play an important role in the accuracy and convergence of the solution. Usage of first order schemes are not recommended since they suffer from numerical diffusion. Second order schemes are well suited for achieving a high level of accuracy, but it takes more iterations for convergence. Therefore, there is a trade off between accuracy and computational effort and the decision depends on the accuracy requirements and the stage of the design. In the case of experimental validation that is going to be made, the level of accuracy required is above the achievable limit of first order schemes and therefore second order schemes are going to be used.

5.3 2-D Calculations

5.3.1 Overview

For the 2-D CFD calculations, it was decided to validate against the experiments made by Wilkinson at the University of Southampton in 1984. [16] Wilkinson stated that the experiments were "aiming to investigate the nature of flow around two dimensional, highly cambered, sail like aerofoil sections with circular masts". He has obtained data in the form of

static pressure distributions for representative ranges of Reynolds numbers, camber ratios, incidence angles, mast diameter/chord ratios, and mast angles. Throughout the experiments, mean camber lines of NACA a=0.8 and NACA 63 foil sections were used. Figure 5.1 shows a snapshot from one of the experiments made by Wilkinson.

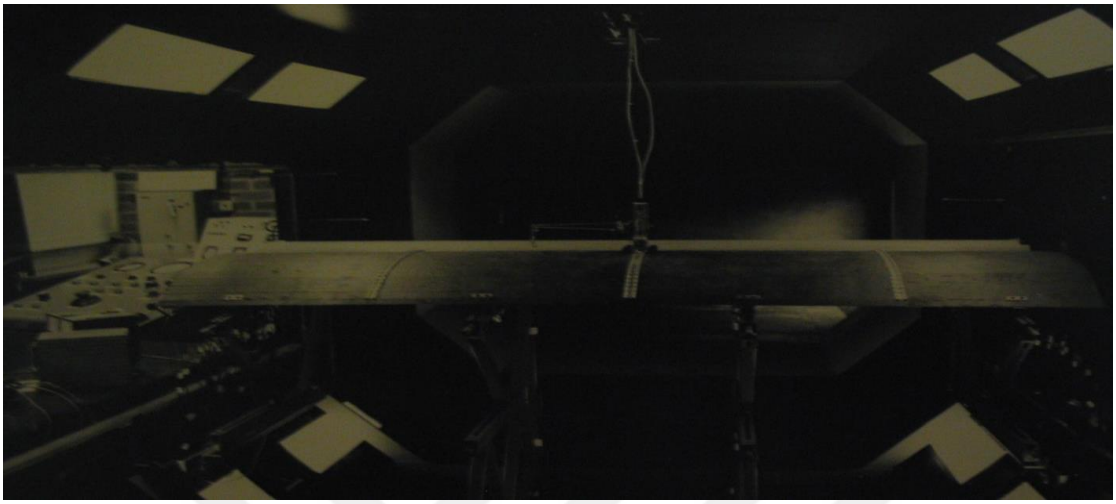

Figure 5.1

The Reynolds numbers that Wilkinson used for the experiments were ranged between $2.0x10^5$ and $1.6x10^6$. It was first anticipated to compare a case with a low Reynolds number, below the turbulent flow threshold of $5.0x10^5$ since in the wind tunnel experiments made with the one metre rig, the Reynolds numbers were below the critical threshold. However, since low Reynolds number flows are problematic within the limitations of available turbulence models, it was decided to select one of the experiments with a Reynolds number which is above the critical threshold.

The experiment chosen for validation had a Reynolds number of $1.0x10^6$, incidence angle of 10 degrees, mast/chord ratio of 0.168, mast angle of 15 degrees and a camber ratio of 0.150. The geometry used was NACA a=0.8 mean camber line. This combination was thought to be representative for the 3-D calculations that were going to be made.

5.3.2 Pre-Processing

Geometry Definition

The coordinates for the NACA a=0.8 mean line were taken from the data supplied by Abbott.[17] It was then modified for 10% camber and exported to Rhinoceros as a text file for further arrangements.

In Rhinoceros, the 15 degrees rotated mast was created and attached to the foil section.

Grid Generation

Sails can be considered as highly thin and cambered aerofoil sections. Modelling of the sails section was achieved by generating a curve without thickness. When the grid is exported to Fluent, the curves without thickness are duplicated and named as “shadow” of the original curve. By this method, two adjacent curves are generated without thickness and the flow negotiates the leading edge around both ways which simulates the actual sail. The procedure is analogous to 3-D sail surfaces as well. An example might be found on figure 5.3.

Previous work done at the University of Southampton by Mr. C. Pashias has been the starting point for the analysis. His personal recommendations demanded the creation of a structured grid for the sail performance analysis problem. A study has been made to develop a strategy for the creation of the structured grid. The creation of a structured grid is highly complex for the combination of a sail section and a rotated mast attachment within the available grid generation software’s tolerances. It was necessary to split the solution domain into parts in order to be able to generate mappable surfaces for structured grid generation. This was done in Rhinoceros owing to the ease of usage of the software. Figure 5.2 shows the solution domain which is divided into mappable faces.

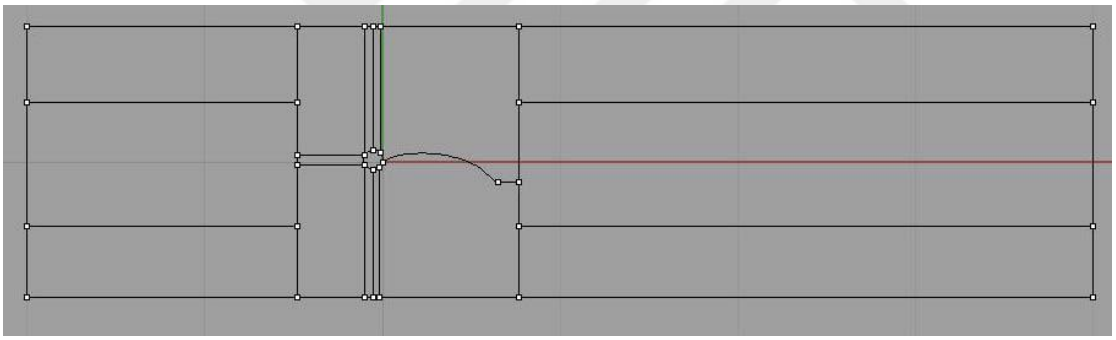

Figure 5.2

The selection for the size of the domain was mainly constrained with the dimensions of the wind tunnel that the experiments were made in. As seen in figure 5.1, the model was attached to the sides of the tunnel in order to eliminate the 3-D effects that would result in induced drag generation. Also, this gave the possibility of analysis in 2-D since there are not any end effects. It has been mentioned in Wilkinson’s project that the wind tunnel data were corrected neither for blockage effects nor streamline curvature effects; therefore the width of the domain was chosen the same as the width of the wind tunnel. The inlet and the outlet were positioned by trail and error; initial calculations with unstructured grids were made to see the influence of their positions on the pressure distributions. They were moved away from the mast and the sail until the influence on the pressure distribution was vanished. Also, for the

outlet, it was aimed to totally capture the wake extending downstream of the sail to prevent reversed flows on the outlet.

Since the data from the experiments were in the form of static pressure distribution, namely pressure coefficients; it was not possible to get the lift and drag coefficients from the experiments for comparison. The solution strategy was decided such that the first aim was to get the exact pressure distribution on the sail. As a result, the first grid was only aimed to capture the pressure distribution and hence lift but not aimed to capture the exact drag which is influenced by the wake downstream. Since the grid density was adjusted for obtaining the exact pressure distribution, it was then decided to record the lift and drag coefficients from the calculations and gradually increase the grid density in the wake region to investigate the variation in the drag coefficient until the optimum grid density is reached. In other words, the grid was going to be refined until the solution becomes grid independent. Figure 5.3 shows the coarse grid generated for initial calculations.

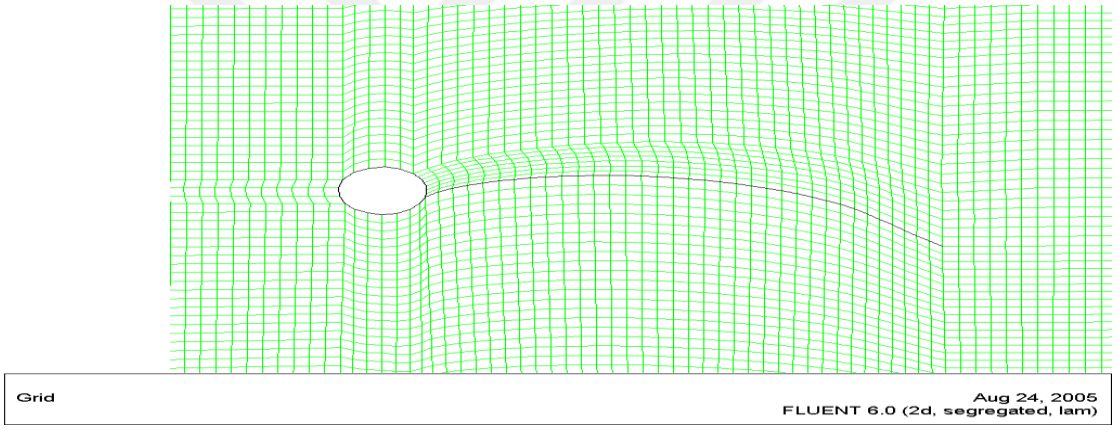

Figure 5.3

5.3.3 The Solution Process

Initial calculations were made with different turbulence models and with different wall treatments to see the variations of pressure distributions. These calculations have shown that the option of enhanced wall treatment is requiring a huge computational effort which can not be readily available for 3-D calculations. Therefore, it was decided to use either turbulence models that do not require any specific wall treatment or wall functions.

Usage of wall functions was seen to be problematic with the particular problem due to the geometry. It has not been possible to manipulate the grid in such a way that the Y+ values would be in a specified range. The Y+ values either dropped below the minimum or were above the maximum recommended by the software vendor. This was mainly due to the separation effects where Y+ values were dropping to zero occasionally. Also, the difference in sizes of the sail section and the mast was making it impossible to have a uniform distribution

of grid that would enable achieving Y+ values in a specified range. This has been reflected to the results as well, none of the turbulence models with wall functions (all the k-ε models and Reynolds Stresses model) have given significant results. Also, it is worth noting that non equilibrium wall functions did not give any better results compared to standard wall functions. After eliminating the above turbulence models, there were two options left; either one of the k-ω models or the Spalart-Allmaras model. Calculations were made with the k-ω models first. These calculations have shown a reasonable agreement with the data available but as mentioned before the sole option of wall treatment for the k-ω models is the enhanced wall treatment which results in increased computational effort that has not paid off in terms of accuracy.

It has been mentioned in section 5.2.1 that Fluent's implementation on the Spalart-Allmaras model enables the usage of coarse meshes for this model. Also, there is not a requirement for an exact range of Y+ values which makes this model more practical. Since there is not a requirement for Y+ values, a systematic wall treatment and grid independence study has been made to obtain the optimum way of wall treatment and grid density for this turbulence model. The hardcopy illustrative images for all the calculations might be found in appendix III.

INITIAL CELLS	FINAL CELLS	MAST MAX Y+	SAIL MAX Y+	CL	CD	CONVERGENCE	ITERATIONS	CP DISTRIBUTION
23899	24454	800	200	1.89	0.17	E-3	230	DIFFERENT
23899	24454	800	200	1.89	0.17	E-4	372	DIFFERENT
23899	25561	400	100	1.94	0.16	E-3	216	DIFFERENT
23899	25561	400	100	1.95	0.16	E-4	303	DIFFERENT
23899	26104	200	100	1.95	0.16	E-3	258	DIFFERENT
23899	26104	200	100	1.95	0.16	E-4	364	DIFFERENT
23899	27175	100	100	1.79	0.18	E-3	315	DIFFERENT
23899	27175	100	100	1.79	0.18	E-4	448	DIFFERENT
23899	31030	50	50	1.60	0.20	E-3	345	AGREES WELL
23899	31030	50	50	1.60	0.20	E-4	557	AGREES WELL
23899	42169	25	25	1.60	0.20	E-3	398	AGREES WELL
23899	42169	25	25	1.60	0.20	E-4	624	AGREES WELL

Table 5.1

This systematic study presented on table 5.1 has shown that the Y+ values should be at most around 50 for obtaining an accurate solution. Lowering the Y+ values further down to first order figures did not result in a difference except for more computational effort. Also, it has been proven that a convergence rate of E-3 is adequate for this problem and solver setting.

The next task was to increase the grid density in the downstream region of the sail to see its influence on the drag values. A prior estimate could not be made about the size of the cells for

the wake region, therefore a study needed to be made. The solution with Y+ values of 50 has been taken as the starting point for this study and with the increased grid quality in the wake region, the drag coefficients were compared with the starting point values.

INITIAL CELLS	FINAL CELLS	CD	CONVERGENCE	ITERATIONS
31030	35518	0.20	E-3	753

Table 5.2

As seen on table 5.2, only one attempt has been made which showed that there is no need to increase the number of cells in the wake region since there has not been a change in the drag coefficient obtained.

Consequently, the final solution has been obtained with 31030 cells with the Spalart-Allmaras turbulence model, with a maximum Y+ value of 50 and with a convergence rate of E-3. The illustrative images of pressure contours, velocity contours and Y+ values for this solution are presented in appendix III. The comparison of pressure coefficients with the experimental data is presented on figure 5.4.

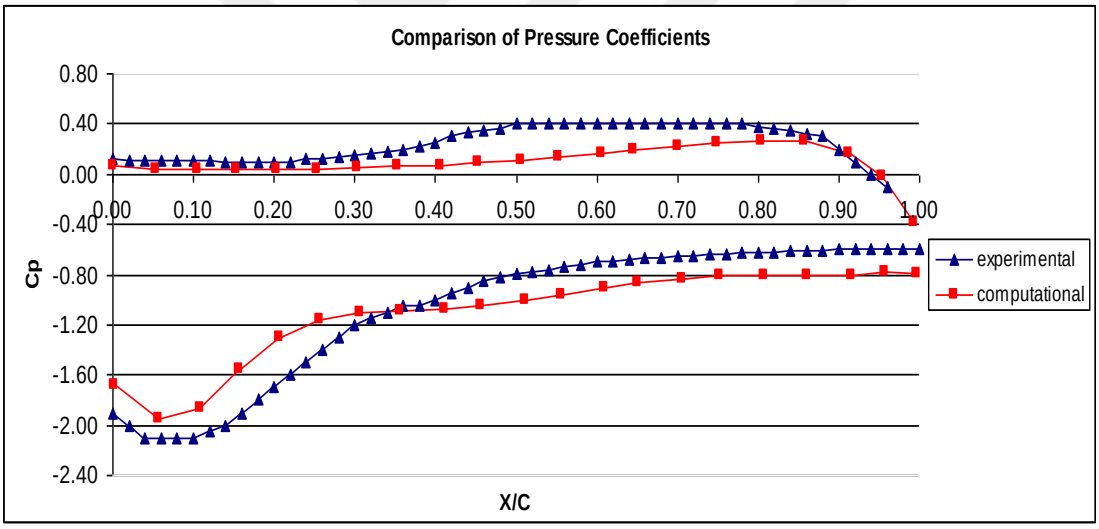

Figure 5.4

The above figure shows that a reasonable agreement has been obtained between the experiments and the numerical calculations. The pressure coefficient plots are not exactly the same but same trends are observed in both.

On the leading edge of the suction side, both experimental and numerical calculations show a region of adverse pressure gradient where the flow is separated due to the existence of the mast. This is also observed in the velocity vectors presented in appendix III. Moving towards the trailing edge, a favourable pressure gradient leads to a re-attachment of the flow. The magnitude of the pressure rise is however more in the experiment compared to numerical

calculations. On the other hand, similar trends in the pressure distributions imply similar separation-reattachment behaviour both experimentally and computationally.

The pressure plots on the pressure sides are more comparable. A possible reason for this is the lesser amount of separation present on the pressure side. As the flow moves towards the trailing edge on the pressure side, there is a pressure rise on both the experiment and numerical calculations. The experimental values in this region are slightly higher than the numerical ones.

The results of the numerical calculations have to be treated with caution in order to make reliable conclusions. In order to make a comparison of pressure coefficient plots, the exact static pressures during the experiments have to be known and these should be input to the numerical calculation. Also, possible sources and magnitude of errors from the experiment have to be taken into account. Such a study has not been made and therefore there is not a quantifiable measure of error associated with the experiment.

This study has concluded that the agreement obtained between the experiment and the numerical calculations are reasonable enough and the differences can be associated to the reasons stated in the above paragraph. This amount of difference is acceptable in the sense that the experiment itself might have some error for which there is not a measure. As a result, it is justified that the results obtained from the 2-D calculations will be the basis of the 3-D calculations which will be done for validating against the experiments made with the one metre rig.

5.4 3-D Calculations

Overview

The 3-D computations are based on validation against experimental results obtained from the one metre yacht experiments. The experiments that will be validated are restricted to seven headings, from 30 to 90 degrees, which were aiming to achieve maximum drive force. As soon as the maximum drive force was achieved, the data were acquired and the sail shapes were recorded digitally.

The acquired data were corrected with the scheme described in chapter 3. It should be noted that the windage drag did not include the rigging since on the CFD calculations the rigging is to be included.

The wind tunnel data will be scaled up arbitrarily to obtain a turbulent flow regime to eliminate low Reynolds number effects on computations. Also, comparisons will be made with the full scale and model data to assess the scaling techniques.

Geometry and Grid Generation

The first step of the 3-D calculations was to prepare the geometry input for mesh generation. The flying shapes that were recorded during wind tunnel experiments were analysed by UK Sails' software ACCUMEASURE. The software basically creates spline sections that can be superposed on to the sail sections and the section data of the sails can be obtained. At each section, the maximum camber, the position of the maximum camber along the chord, the camber at 15% and 75% of the chord and the twist can be obtained. These data then are dimensionalised according to the sail plan and joined to generate the sail surfaces. Figure 5.5 shows a snapshot from the program.

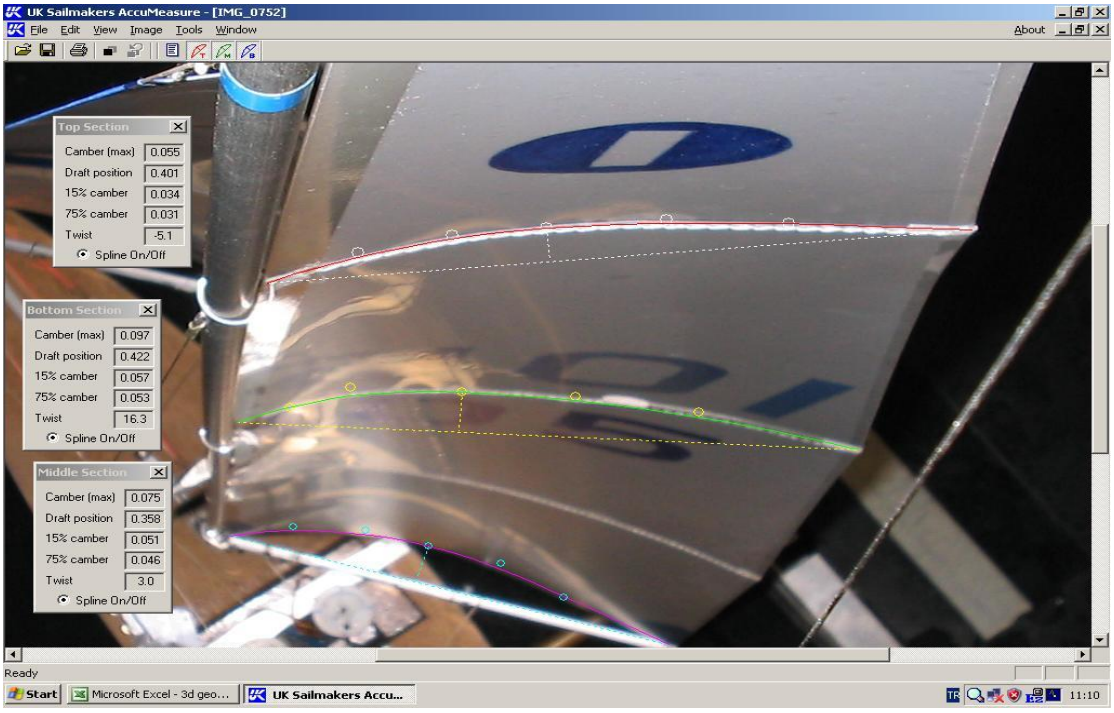

Figure 5.5

The shots of headings of 30 and 90 degrees were not taken from the correct perspective and therefore these cases could not be analysed.

It is worth noting that assumptions were deemed to be made during this process. The fore sail's boom was the main problem and there was not a measure of twist of the fore sail sections with the given twist angles since the coordinates that they lie on the space was not known. The boom-rail attachment was assumed to be 20% of the boom length away from the fore luff at the foot and this point was assumed to be the centre of all the rotations of the sail sections. Also, there was not a measure of mast bending, it was assumed to be non deformed at all cases.

One important difficulty that might possibly lead to errors is the fact that the software vendor recommends the usage of aerial images in order to prevent deviations in the analysis of the sail section due to different perspectives while shooting the pictures. This could not be

achieved with the available equipment and therefore the pictures were taken manually by a person inside the tunnel which lead to different perspectives at all cases and the existence of the person inside the tunnel altered the flow on the sails which might be observed from the shots.

The sail surfaces and the mast were created in Rhinoceros and they were exported to GAMBIT as iges files. It was mentioned previously that the Reynolds numbers of the model were below the turbulence threshold and hence the model would be scaled up to eliminate the low Reynolds number effects that are problematic within the available turbulence modelling schemes in Fluent. Therefore, a scale factor of 20 was used arbitrarily to assess the performance of a full scale yacht with a turbulent flow regime. After scaling up the geometry, the solution domain was created. The decision of the extents of the domain was different from the 2-D case since the 2-D case was just based on comparison of the wind tunnel experiments results with CFD. However, the basis of the 3-D calculations is performance estimation of a full scale yacht which yields the simulation of real operating conditions rather than simulating a constrained environment like a wind tunnel. Reference 1 was a good starting point for the selection of the domain size. For an America's Cup yacht which is similar in size with the full scale boat concerned, the domain size in reference 1 was selected as 300 metres long, 300 metres wide and 80 metres deep. It is worth noting that the computations in reference 1 were based on off wind sails with huge spinnakers and the massive wake size demands such a huge computational domain. In the computations that were to be done, only main and fore sails were going to be used on mainly upwind conditions, therefore it was decided to use a smaller domain which is big enough not to influence the solution. As a result, the domain was decided to be 200 metres long, 150 metres wide and 70 metres deep. This was also necessary in order to reduce the number of cells since the computational resources were limited.

After the creation of the solution domain, the boundary conditions were assigned. The sails and the mast were set as walls with no-slip whereas the sides and the top of the domain were set as free-slip walls with zero shear in order to eliminate the creation of a boundary layer. The inlet was set as a velocity inlet, and the outlet as outflow. The bottom of the domain which is attached to the bottom of the mast was set as a symmetry plane to be able to make use of the symmetry condition and the mirror-image concept.

The most challenging part of the pre-processing was the mesh generation. Within the available meshing schemes, a structured mesh could not be generated for any case. As a result, unstructured meshes were generated for all the cases. This resulted in twice the number of cells for the same spacing and hence more computational effort which might result in an

inaccurate wall treatment depending on the capacity of memory of the computer station that is going to be used for the computations.

The main sail mast attachment and the existence of the fore sail in close proximity were preventing the control of the mesh size. In order to apply the suitable wall treatment, the mesh sizes on the sails and the mast were deemed to be kept small. This was impossible within the available mesh generation software. When the mesh size was kept very small compared to the size of the geometry, the mesher was not able to mesh the whole geometry with the specified spacing and there were holes left on the sails that were not meshed. Therefore, the sails were meshed with the spacing allowed by the software and it was decided to use the adaption tool of Fluent later on during solution.

Another problem while meshing was the gap between the fore sail and the mast-main sail combination. Since the mesh sizes on the sails and the mast were kept as small as possible, it was impossible to use the same spacing in the domain which surrounds the sails since it led to errors regarding lack of memory on the computer. Therefore, the surrounding region had to be meshed with a relatively larger spacing and the manipulation of the spacing was extremely difficult. As a result, the sails and the mast were meshed with 0.1 metres spacing and at the extremities of the domain, the cell size was chosen to be 3 metres. This decision was a necessity since decreasing the cell size at the extremities ended up in excessive number of cells. The final mesh had around one million tetrahedral elements and it was assumed that it would be possible to have adequate memory for the final mesh after adaption.

The Solution Process

The solution scheme was kept the same as the 2-D calculations. Same turbulence models, same discretization schemes, same solver setting were used throughout the 3-D calculations. The computations were carried out on an AMD 64 bit double processor workstation with 1 GB of memory.

Initial calculations showed that the Y+ values were not in the desired range which was expected during grid generation. The Y+ values were around 300 and they needed to be reduced to 50 for a suitable wall treatment according to the 2-D study that was made. An adaption yielded 2 million cells with Y+ values around 150. Since this was still not enough, the next adaption resulted in about six million cells and the Y+ values were still not in the desired range. At this point, the computational resources were not adequate to get a solution and the error message resulting from lack of memory has lead to the necessity of using the solutions with 2 million cells and Y+ values of 150 for all the cases.

6. COMPARISON OF RESULTS AND CONCLUSIONS

It was known prior to the computation process that the level of confidence associated with the results would not be as high as it was anticipated beforehand mainly due to the unsuitable wall treatment being applied as a necessity. However, the magnitude of error of the results could be estimated with the aid of the 2-D study that was made. The study shows that for Y+ values between 100 and 200, the percentage of error for lift coefficients should approximately be 20 percent whereas for the drag coefficients, it should be approximately 25 percent.

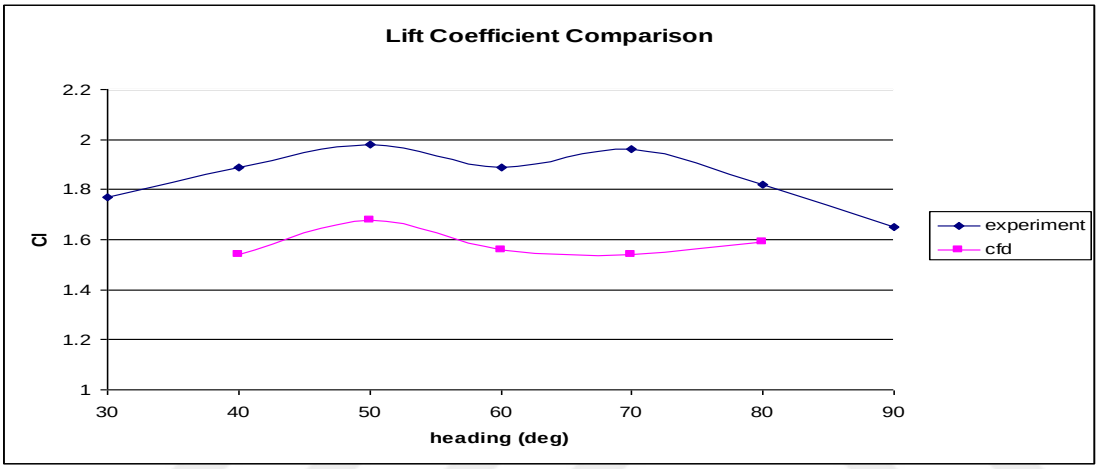

Figure 6.1

Figure 6.1 shows the comparison of lift coefficients and the percentage of error is about 20% which was estimated. The curves show very similar trends and these together lead to the fact that a suitable wall treatment would yield closer lift coefficients. Also, there might be high Reynolds number effects which influence the achievable lift coefficient which is hard to quantify. [11] This in turn depends on the foil type and published data for sails could not be found.

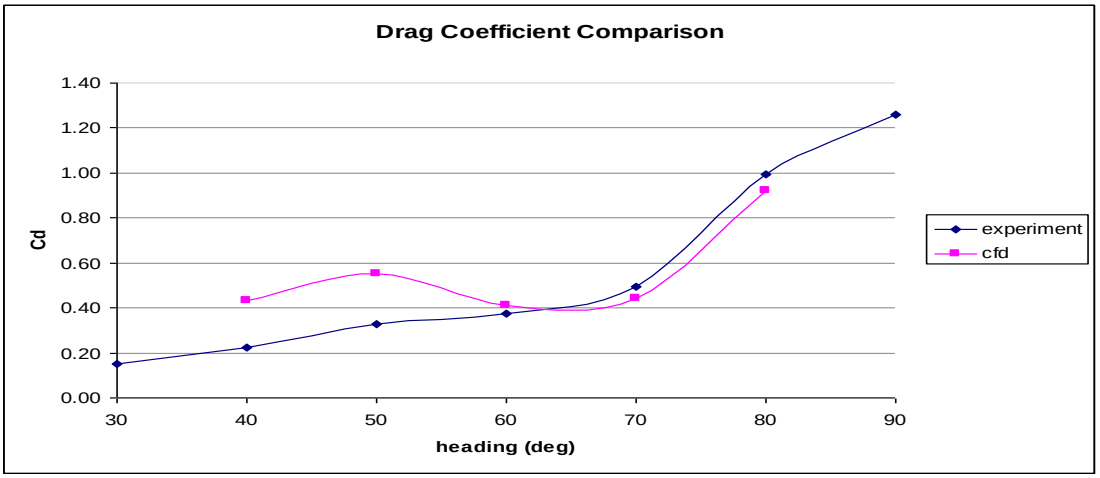

Figure 6.2

Figure 6.2 shows the comparison of drag coefficients and the figure can be divided into two regions where the calculated drag coefficients are about half of the experimental ones and a region where the coefficients agree reasonably with each other. A possible reason for this trend might be the strong interaction of sails in close hauled conditions. Since the sails are sheeted close to the centre line in close hauled conditions, there is a strong interaction between the sails named as slot effect; and the grid sizing is not small enough to capture this interaction that changes the efficiency of the sails. This interaction vanishes as the heading is increased, since the sails are sheeted away from the centre line. At these conditions, there is a reasonable agreement of drag coefficients, but the Y+ values are not in the specified range and this leads to a deviation from the experimental values. The figures below show the differences between Y+ values of the 2-D and 3-D computations.

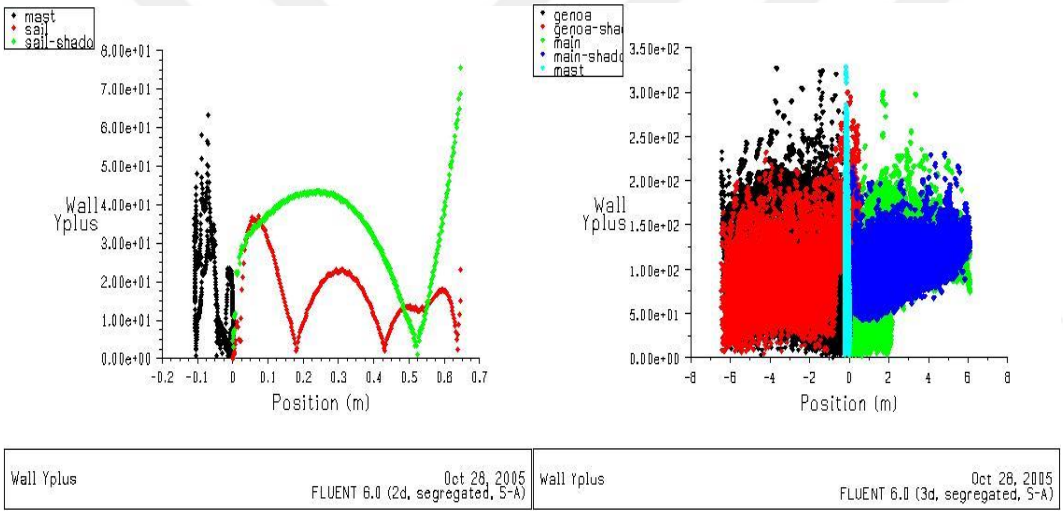

Figure 6.3

According to the figure above, a high lever of accuracy and confidence can not be associated to the 3-d calculations made since the most influential parameters could not be kept in the required range. An unsuitable wall treatment changes the results dramatically as it was seen on the 3-D results obtained.

Another point to note is the poor grid quality around the mast. At 2-D calculations, the region around the mast and the main sail attachment point was consisting of a highly fine grid that would capture the salient features of the flow. This includes the region inside the boundary layer for a suitable wall treatment and the region outside the boundary layer surrounding the mast where the gradients of velocity are high. This could not be achieved in 3-D calculations and it is thought that this might have influenced the results. Figure 6.4 shows the grid quality difference between the 2-D and 3-D calculations.

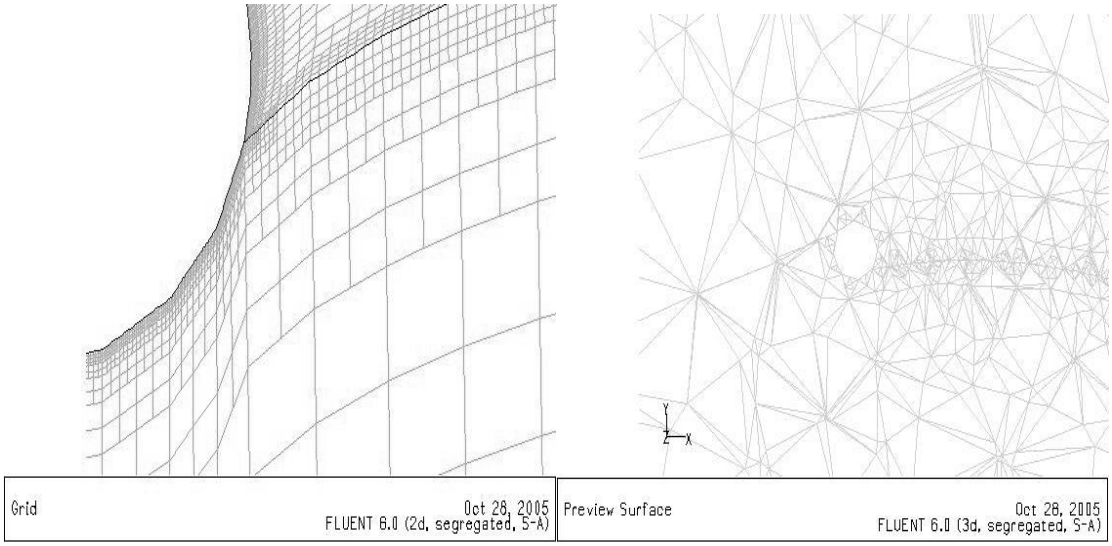

Figure 6.4

Apart from wall treatment and mesh size deficiencies, the necessity of using unstructured meshes for the computations might be a source of error since all the 2-D investigations were made with structured meshes. The most suitable settings for the structured mesh and the unstructured mesh might eventually be different. These include the mesh density, wall treatment, convergence criteria, discretisation schemes and it might even include the turbulence model being used. A study has not been made for unstructured meshes and this also reduces the level of confidence.

The pressure contours, velocity contours, convergence history plots and Y+ plots of all the 3-D computations might be found in appendix IV.

Conclusions

RANS solvers have shown to be a possible tool for performance prediction of sailing yachts for the future, but as yet they suffer from couple of difficulties. The main difficulty is the requirement of powerful computational tools that are not readily available in relatively low budgeted office environments. This requirement is mainly due to the enhanced wall treatment that needs to be applied with the turbulence models that are applicable to the problem. The turbulence models that use wall functions and hence relatively coarser grids are not applicable to the sail performance prediction problem as yet. These models need to be developed to give better results in separated flow regimes. The mesh generation softwares need to be developed mainly in terms of mesh generation techniques. Structured meshes are thought to give better results for the sail performance analysis problem since more control can be achieved over the grid in regions of interest.

Apart from the mentioned aspects, the sail performance prediction demands the flying sail shapes at each condition of sailing. Reference 1 states that a software coupling a structural

finite element code to a CFD code is under development. It is not developed as yet to the extent required by the industry and it is not available for use by the industry. The estimation of the flying shape is rather difficult and problematic, also the number of cases to be assesses is high owing to the numerous variables that need to be changed. This requires a lot of effort and time; and the results are not as accurate as they are required to be. As a result of these, CFD tools are only being used for high budgeted applications for the time being. Quoting reference 18: “There currently exists a wide range of Computational Fluid Dynamics (CFD) tools for the numerical simulation of aerodynamic and hydrodynamic flows. Such tools are finding increasing use in a wide range of application areas. For example, in the aerospace and automotive industries, CFD methods have been successfully integrated into the design process. More recently, the introduction of these tools into the marine industry has been motivated in part by their application to racing yacht design (Larsson, 1990; Milgram, 1998) For the America’s Cup and Volvo Ocean races, where syndicate budgets can reach US$ 100 million, the use of CFD tools is becoming widespread”. This reference explains the situation clearly, stating that the use of RANS codes is restricted to high budget projects for now. In addition, they are being used for academic purposes. The integration of these tools into an ordinary design office environment is the challenging task for the time being and the possible future developments in the softwares and computational tools will aid this integration process.

REFERENCES

1. Richter H., Horrigan K., Braun J.B.; "Computational Fluid Dynamics for Downwind Sails"

2. Claughton A., Shenoi A., Wellicome J.; "Sailing Yacht Design – Theory"
Addison Wesley Longman Limited, Essex, 2002

3. Marchaj C.A.; "Aero-Hydrodynamics of Sailing"
Adlard Coles Nautical, London, 2000

4. Houghton E.L., Carpenter P.W.; "Aerodynamics for Engineering Students"
Butterworth-Heinemann, Burlington, 2003

5. Larsson L., Eliasson R.E.; "Principles of Yacht Design"
McGraw-Hill, Great Britain, 2000

6. Depledge B. H.; "An Investigation into the use of High Roach Main Sails on International America's Cup Class Yachts"
MEng Project, University of Southampton, 2005

7. "Yacht Experimental Techniques, Wind Tunnel Testing Lecture Notes"
University of Southampton, 2004

8. Hearn G. E.; "High Performance Craft Lecture Notes"
University of Southampton, 2004

9. Campbell I.; "Wind Tunnel Testing of Sailing Yacht Rigs"

10. Ranzenbach R., Mairs C.; "Wind Tunnel Testing of Offwind Sails"
The 14th Chesapeake Sailing Yacht Symposium

11. Pope A., Barlow J. B., Rae W. H. JR.; "Low-Speed Wind Tunnel Testing"
John Wiley & Sons, New York, 1999

12. Campbell I.; Personal Communication

13. http://www.lmnoeng.com/Flow/GasViscosity.htm

14. "Advanced Turbulence Notes"
Fluent Europe LTD, Sheffield, 2004

15. WS Atkins Consultants, "Best Practice Guidelines for Marine Applications of CFD"

16. Wilkinson S.; "Partially Separated Flow Around Masts and Sails"
PhD Project, University of Southampton, 1984

17. Abbott I. H., Von Doenhoff A. E.; "Theory of Wing Sections"
Courier Dover Publications, New York, 1959

18. Cowles G., Parolini N., Sawley M. L.; “Numerical Simulation using RANS-based Tools for America’s Cup Design”
The 16th Chesapeake Sailing Yacht Symposium, Maryland, March 2003

APPENDICES

APPENDIX I WIND TUNNEL RAW DATA

APPENDIX II SAIL PLAN DRAWINGS USED FOR 3-D COMPUTATIONS

APPENDIX III TWO DIMENSIONAL COMPUTATIONAL PRESSURE DISTRIBUTION, VELOCITY CONTOURS, VELOCITY VECTORS, PRESSURE CONTOURS, Y+ PLOTS, CONVERGENCE HISTORY PLOTS

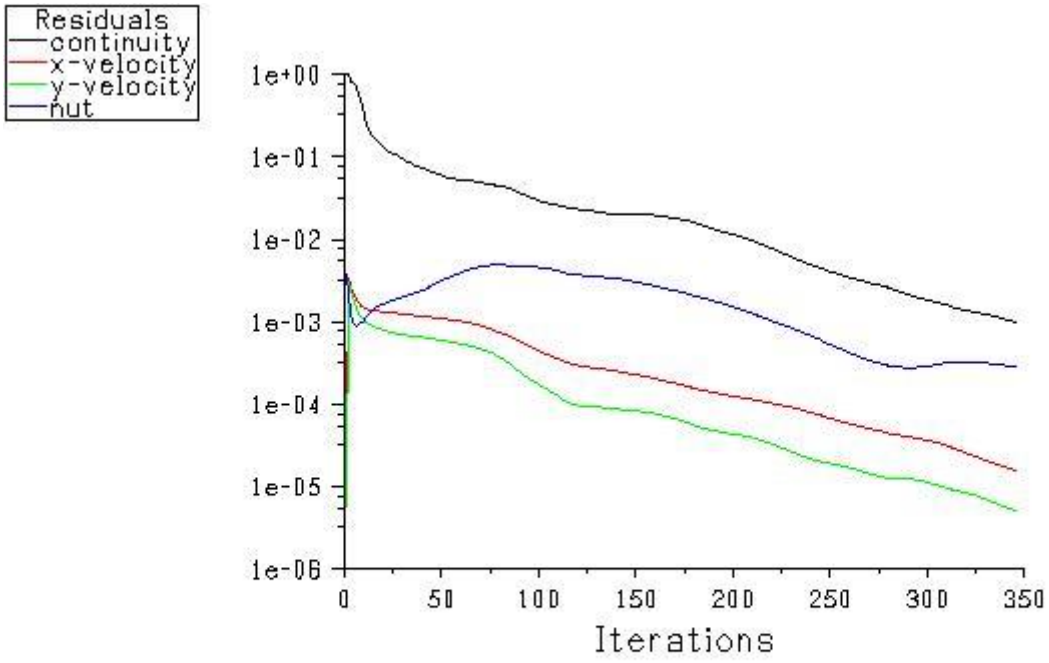

Scaled Residuals

Oct 28, 2005
FLUENT 6.0 (2d, segregated, S-A)

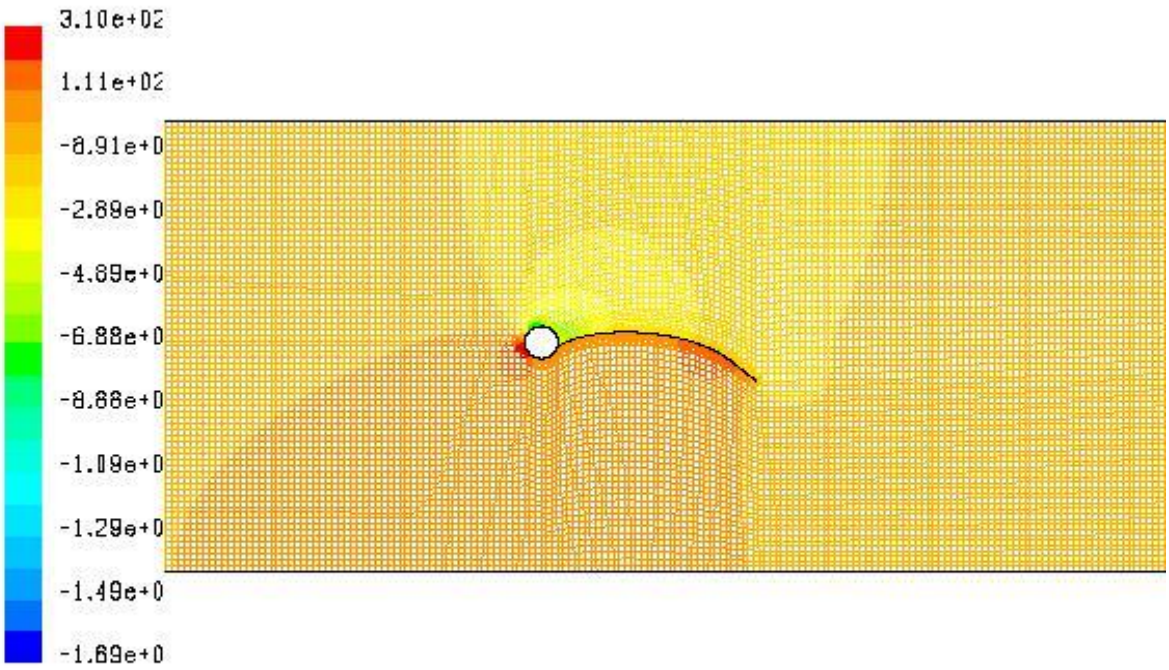

Contours of Static Pressure (pascal)

Oct 28, 2005
FLUENT 6.0 (2d, segregated, S-A)

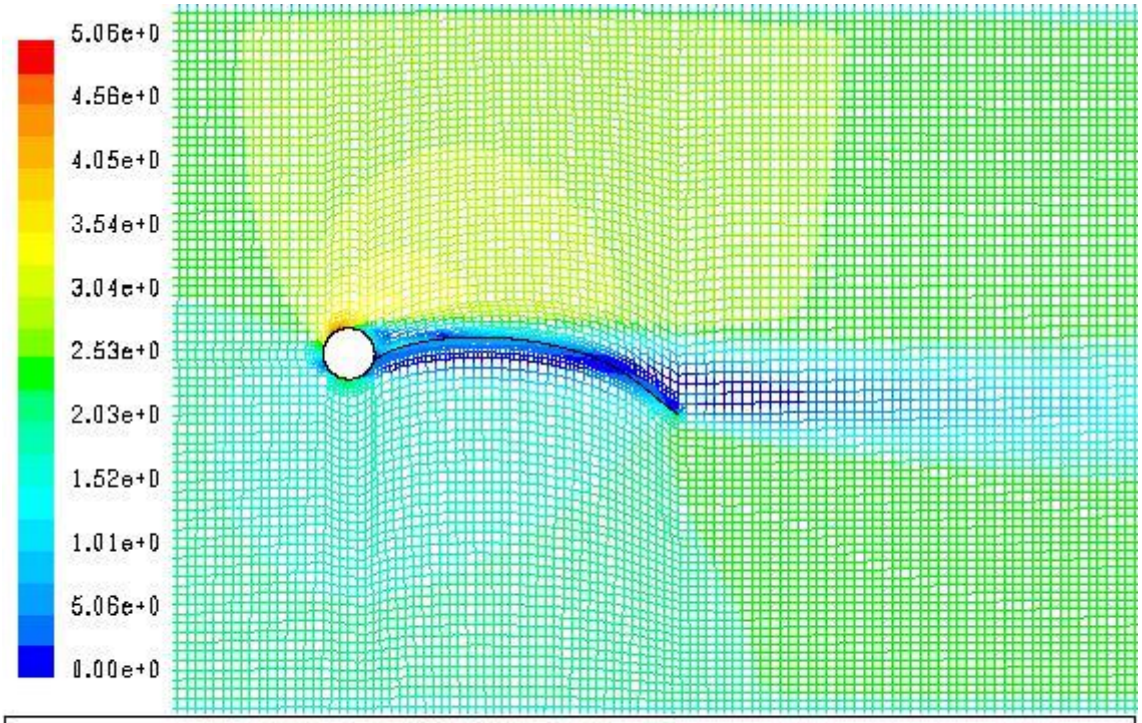
5.06e+0
4.56e+0
4.05e+0
3.54e+0
3.04e+0
2.53e+0
2.03e+0
1.52e+0
1.01e+0
5.06e+0
0.00e+0
Contours of Velocity Magnitude (m/s)
Oct 28, 2005
FLUENT 6.0 (2d, segregated, S-A)

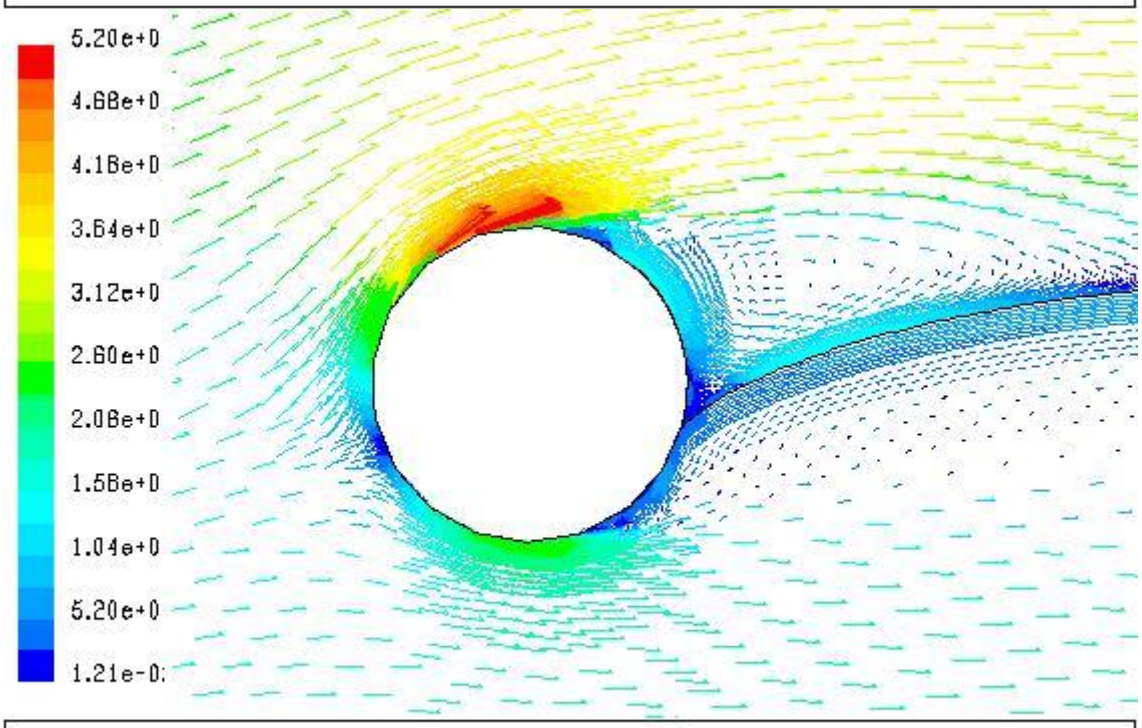
5.20e+0
4.68e+0
4.16e+0
3.64e+0
3.12e+0
2.60e+0
2.08e+0
1.56e+0
1.04e+0
5.20e+0
1.21e-0:
Velocity Vectors Colored By Velocity Magnitude (m/s)
Oct 28, 2005
FLUENT 6.0 (2d, segregated, S-A)

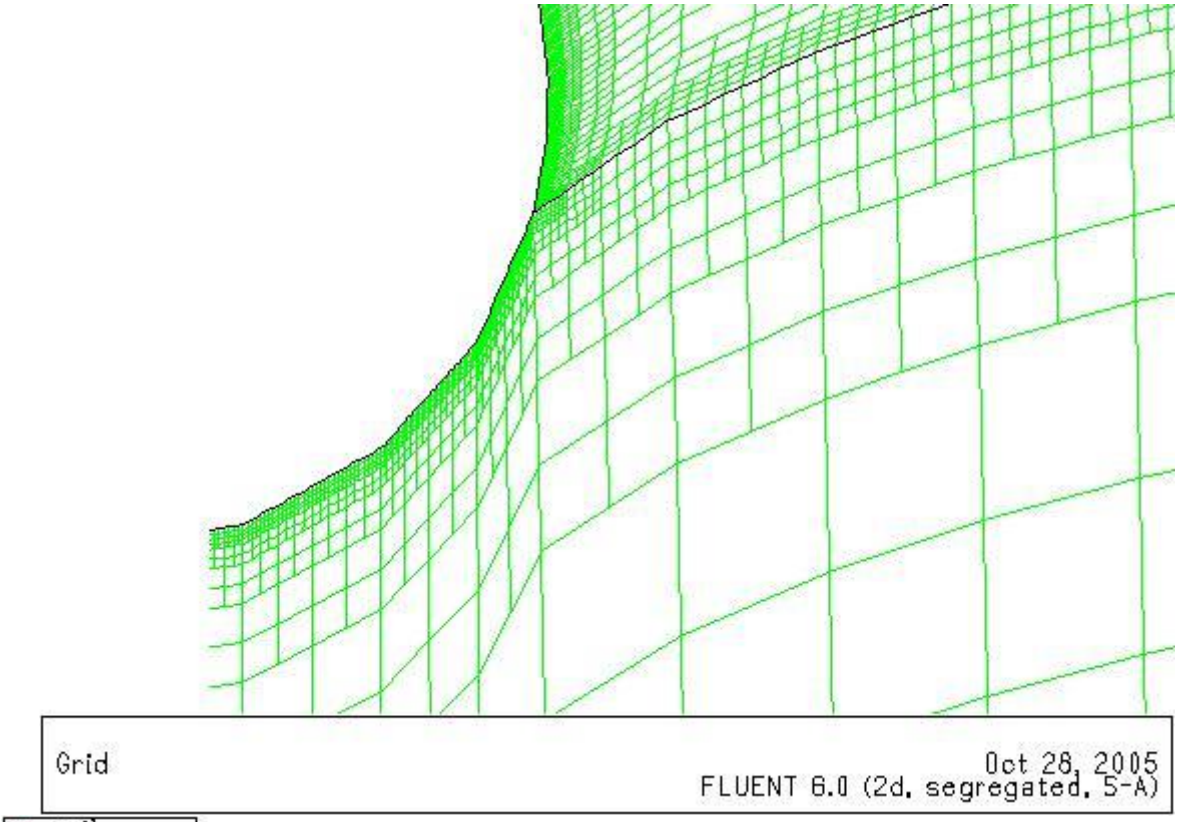
Grid
Oct 28, 2005
FLUENT 6.0 (2d, segregated, S-A)

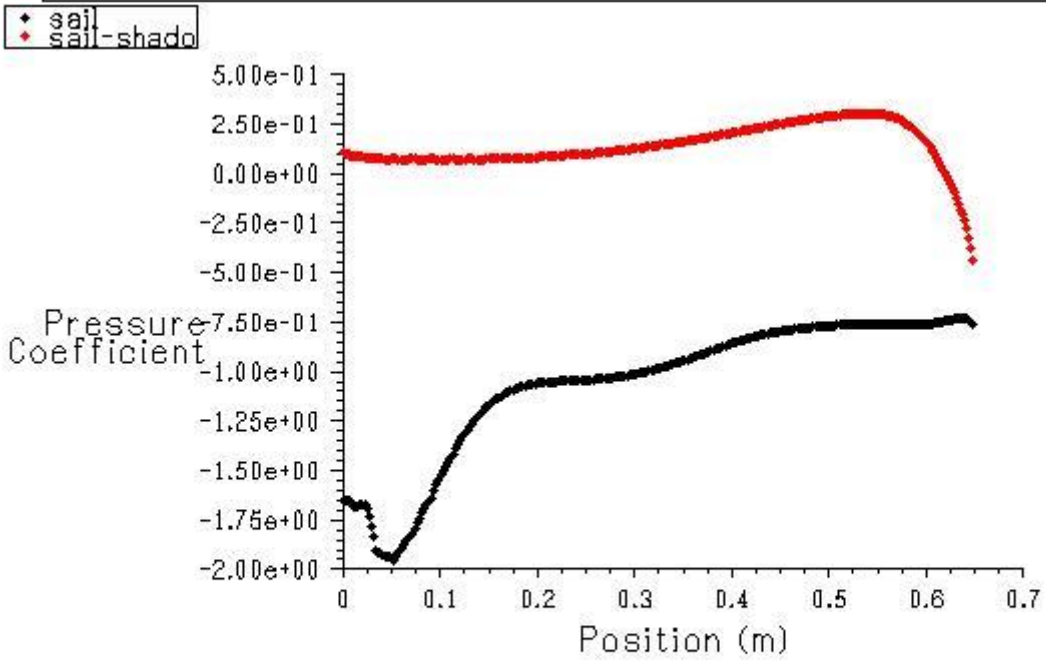
sail
sail-shado
5.00e-01
2.50e-01
0.00e+00
-2.50e-01
-5.00e-01
-7.50e-01
-1.00e+00
-1.25e+00
-1.50e+00
-1.75e+00
-2.00e+00
Pressure Coefficient
0
0.1
0.2
0.3
0.4
0.5
0.6
0.7
Position (m)
Pressure Coefficient
Oct 28, 2005
FLUENT 6.0 (2d, segregated, S-A)

APPENDIX IV THREE DIMENSIONAL VELOCITY CONTOURS, PRESSURE CONTOURS, Y+ PLOTS, CONVERGENCE HISTORIES

β=40 degrees

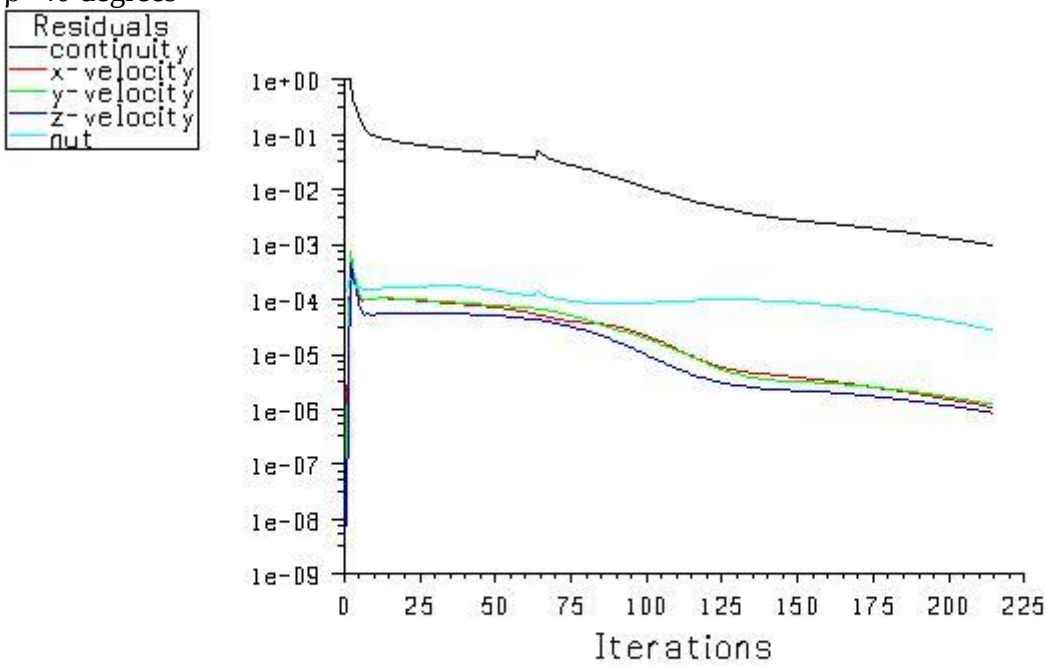
Residuals
continuity
x-velocity
y-velocity
z-velocity
nut
1e+00
1e-01
1e-02
1e-03
1e-04
1e-05
1e-06
1e-07
1e-08
1e-09
0
25
50
75
100
125
150
175
200
225
Iterations

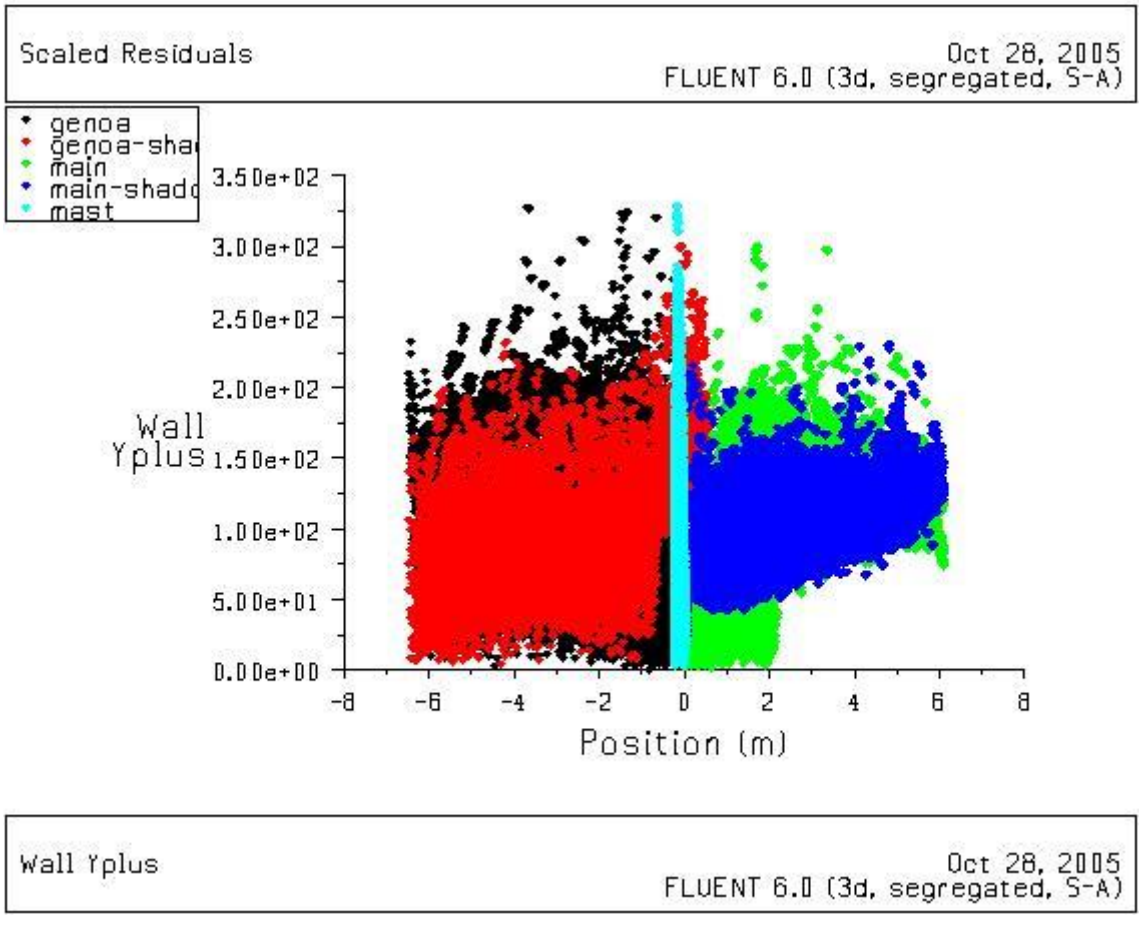
Scaled Residuals
Oct 28, 2005
FLUENT 6.0 (3d, segregated, S-A)
genoa
genoa-sha
main
main-shadc
mast
3.50e+02
3.00e+02
2.50e+02
2.00e+02
1.50e+02
1.00e+02
5.00e+01
0.00e+00
Wall Yplus
-8
-6
-4
-2
0
2
4
6
8
Position (m)

Wall Yplus
Oct 28, 2005
FLUENT 6.0 (3d, segregated, S-A)

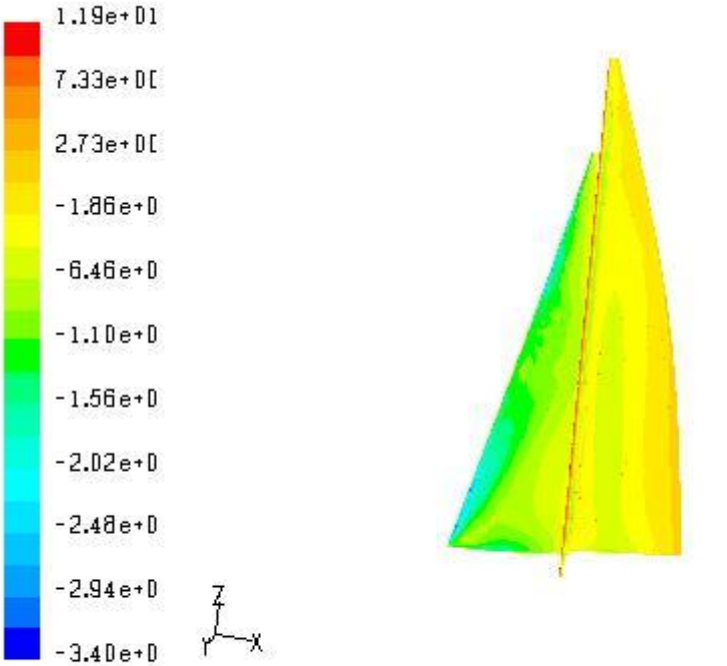

Contours of Static Pressure (pascal)

Oct 28, 2005
FLUENT 6.0 (3d, segregated, S-A)

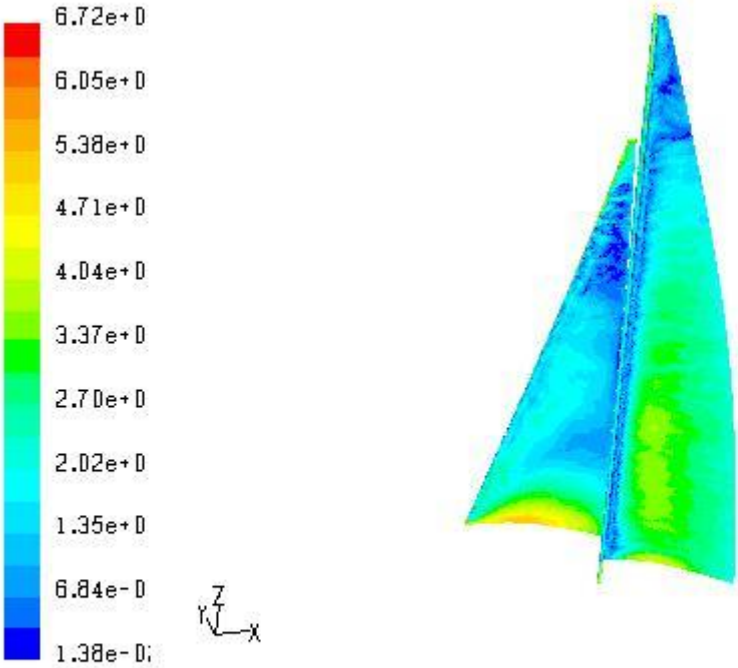

Contours of Velocity Magnitude (m/s)

Oct 28, 2005
FLUENT 6.0 (3d, segregated, S-A)

β=50 degrees

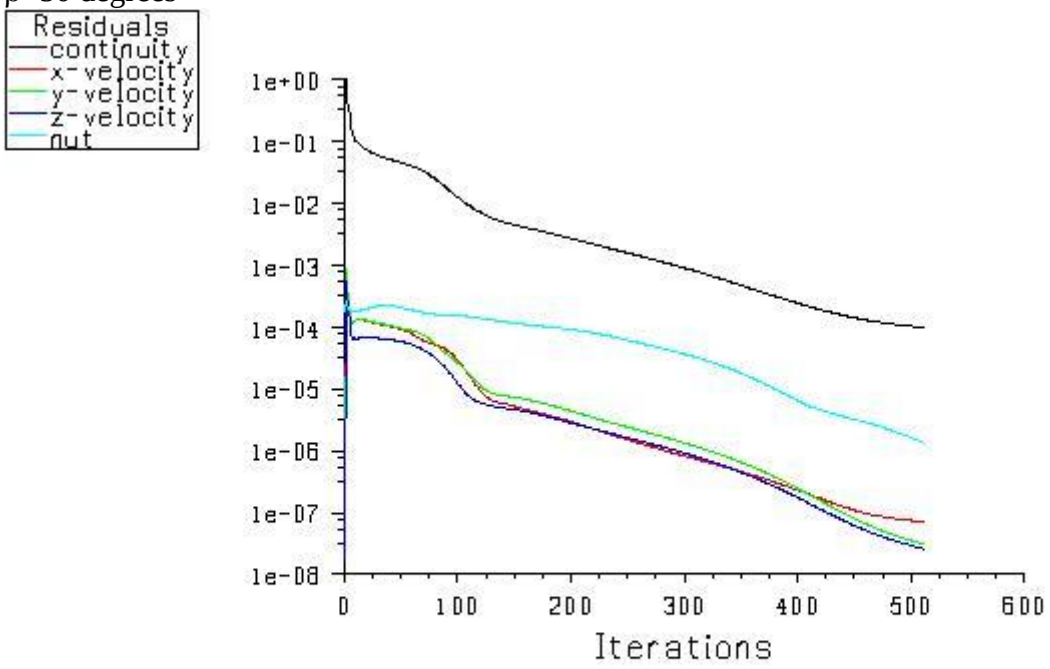
Residuals
continuity
x-velocity
y-velocity
z-velocity
nut
1e+00
1e-01
1e-02
1e-03
1e-04
1e-05
1e-06
1e-07
1e-08
0
100
200
300
400
500
600
Iterations

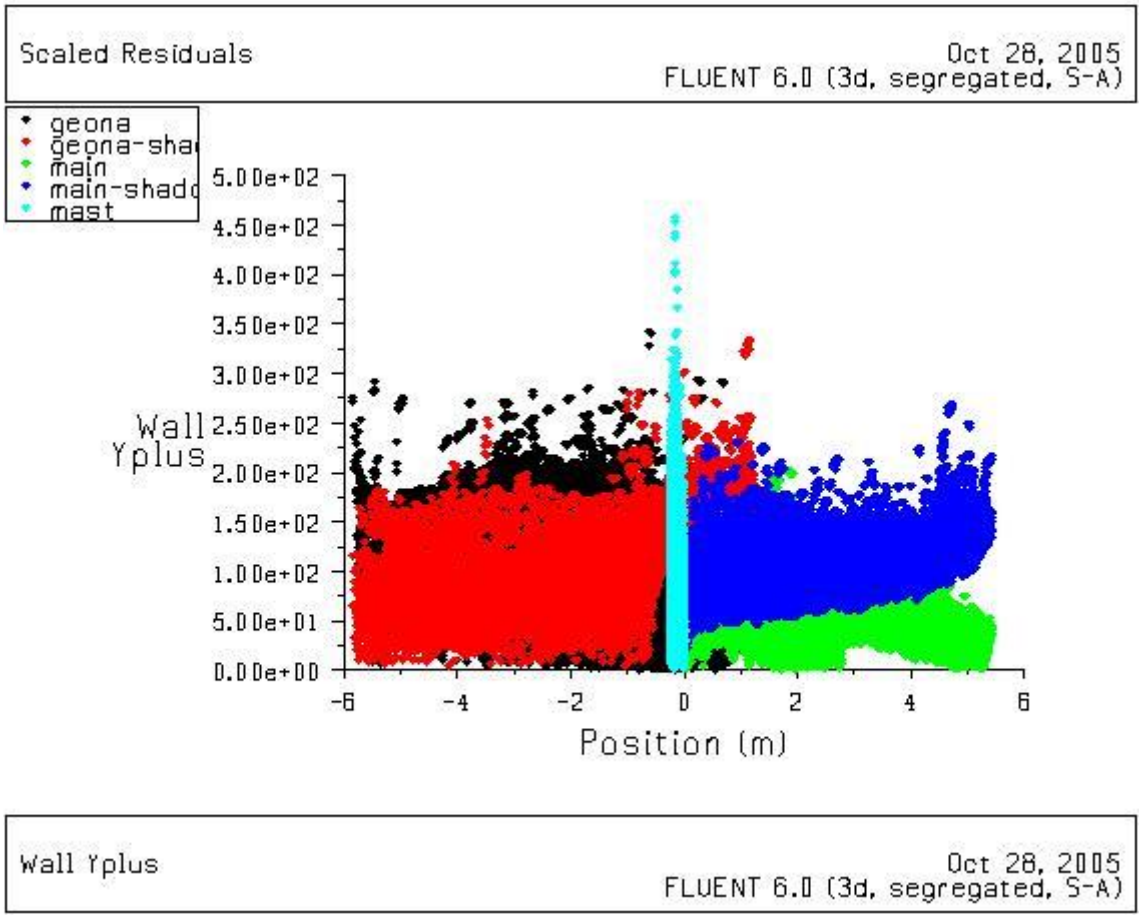
Scaled Residuals
Oct 28, 2005
FLUENT 6.0 (3d, segregated, S-A)
geona
geona-sha
main
main-shadc
mast
5.00e+02
4.50e+02
4.00e+02
3.50e+02
3.00e+02
2.50e+02
2.00e+02
1.50e+02
1.00e+02
5.00e+01
0.00e+00
Wall Yplus
-6
-4
-2
0
2
4
6
Position (m)

Wall Yplus
Oct 28, 2005
FLUENT 6.0 (3d, segregated, S-A)

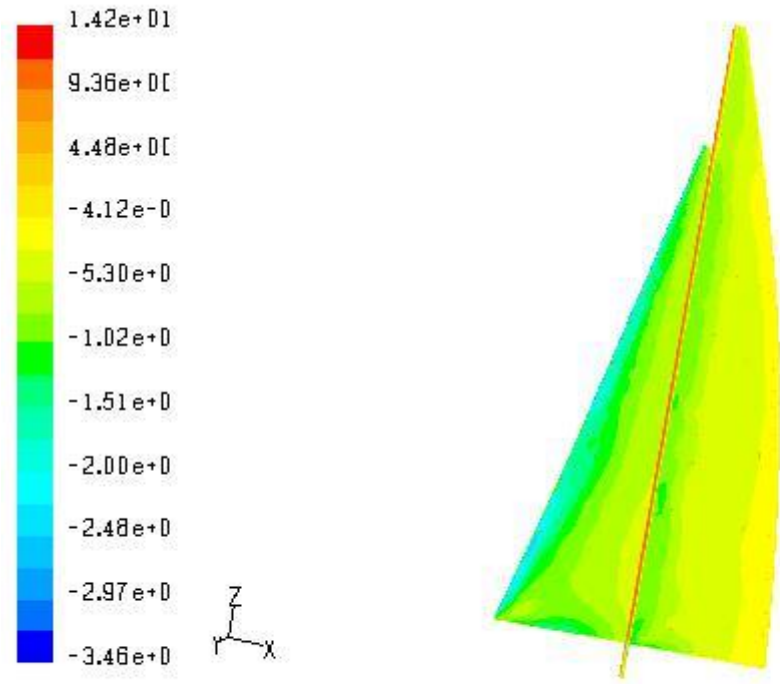

Contours of Static Pressure (pascal)

Oct 28, 2005
FLUENT 6.0 (3d, segregated, S-A)

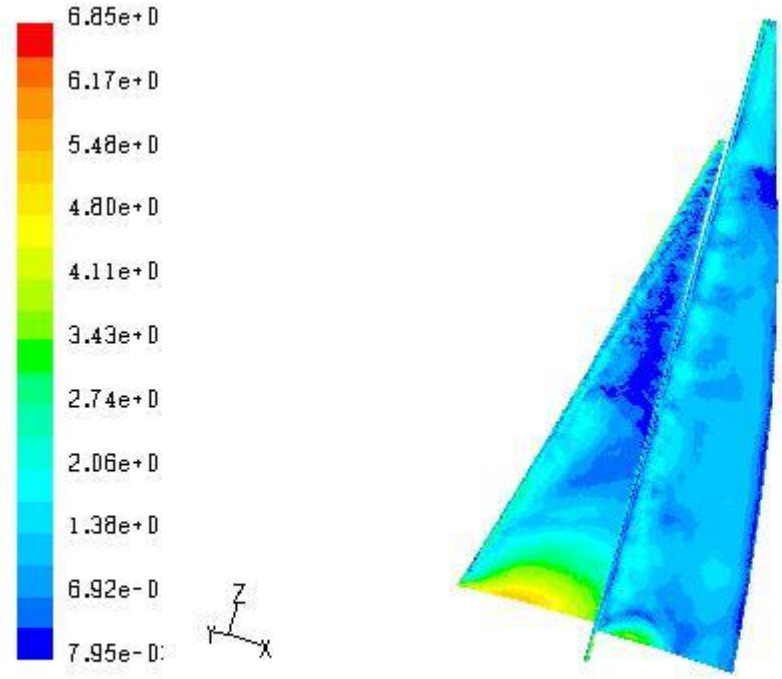

Contours of Velocity Magnitude (m/s)

Oct 28, 2005
FLUENT 6.0 (3d, segregated, S-A)

β=60 degrees

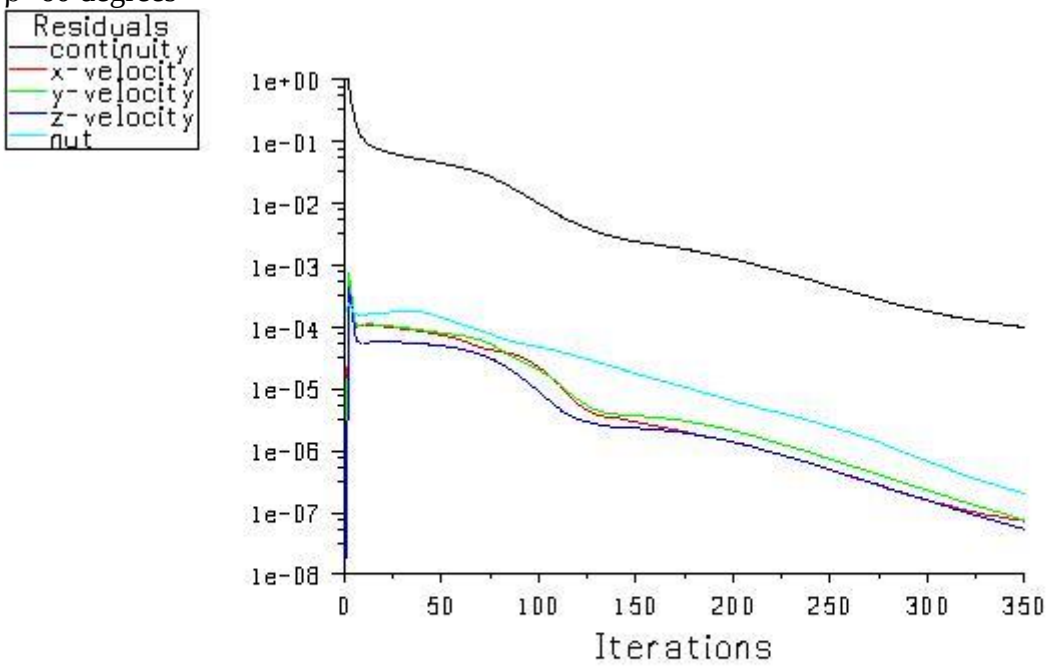
Residuals
continuity
x-velocity
y-velocity
z-velocity
nut
1e+00
1e-01
1e-02
1e-03
1e-04
1e-05
1e-06
1e-07
1e-08
0
50
100
150
200
250
300
350
Iterations

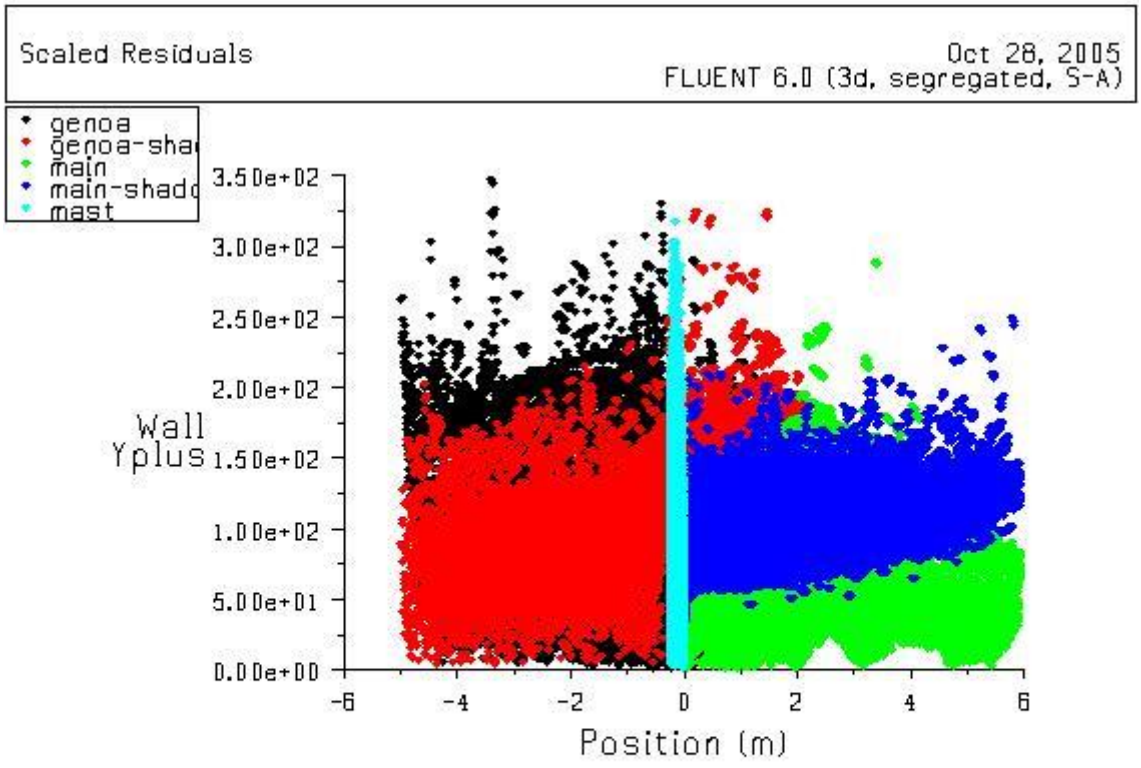
Scaled Residuals
Oct 28, 2005
FLUENT 6.0 (3d, segregated, S-A)
genoa
genoa-sha
main
main-shadc
mast
3.50e+02
3.00e+02
2.50e+02
2.00e+02
1.50e+02
1.00e+02
5.00e+01
0.00e+00
Wall Yplus
-6
-4
-2
0
2
4
6
Position (m)


Wall Yplus
Oct 28, 2005
FLUENT 6.0 (3d, segregated, S-A)

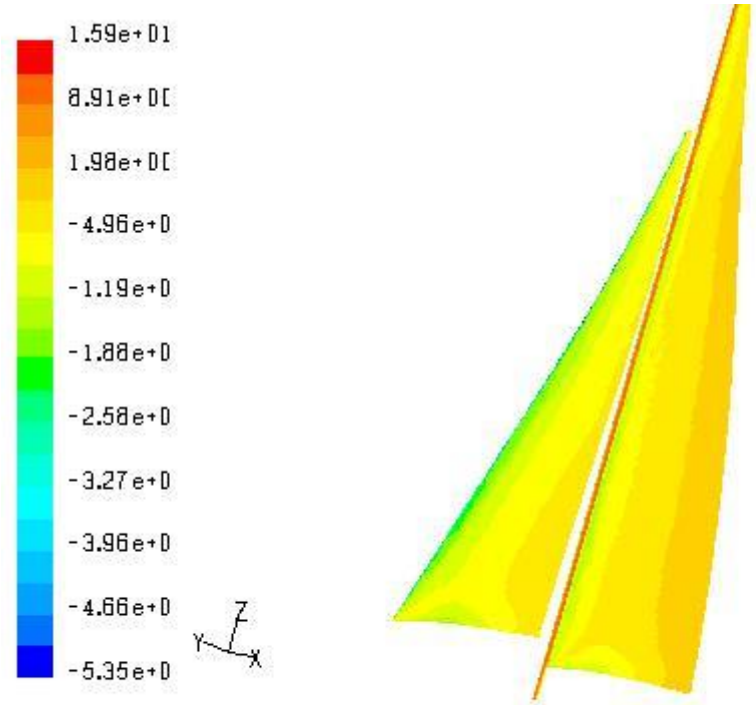

Contours of Static Pressure (pascal)

Oct 28, 2005
FLUENT 6.0 (3d, segregated, S-A)

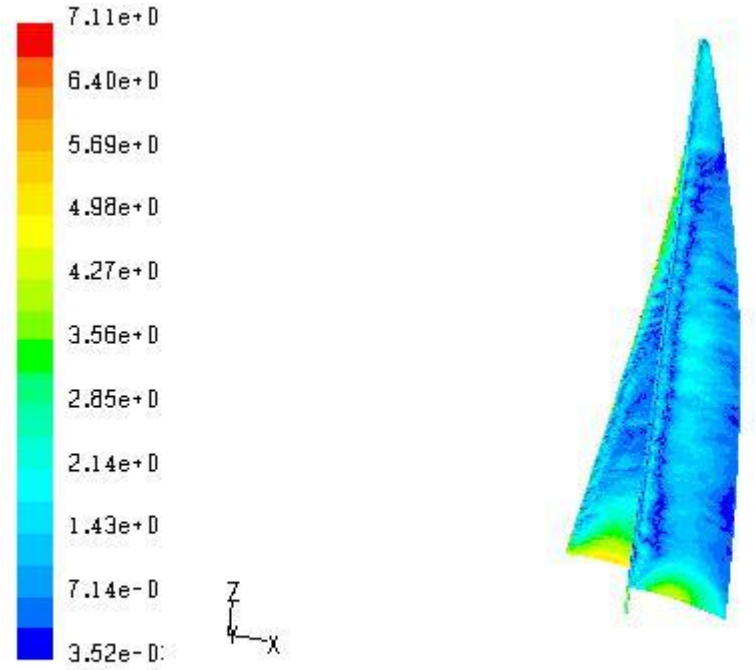

Contours of Velocity Magnitude (m/s)

Oct 28, 2005
FLUENT 6.0 (3d, segregated, S-A)

β=70 degrees

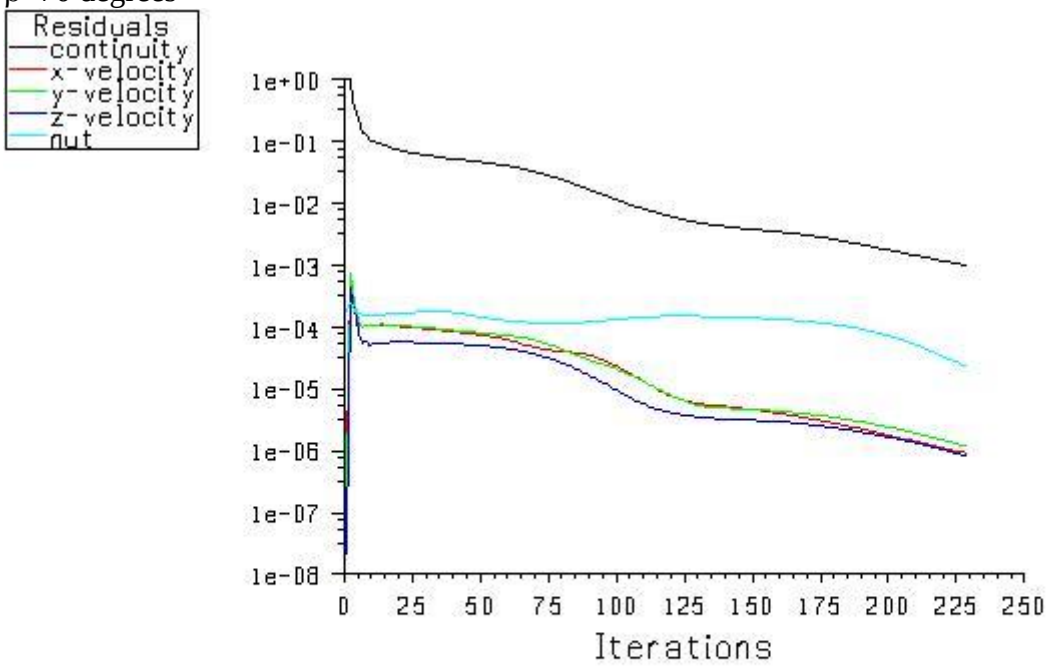
Residuals
continuity
x-velocity
y-velocity
z-velocity
nut
1e+00
1e-01
1e-02
1e-03
1e-04
1e-05
1e-06
1e-07
1e-08
0
25
50
75
100
125
150
175
200
225
250
Iterations

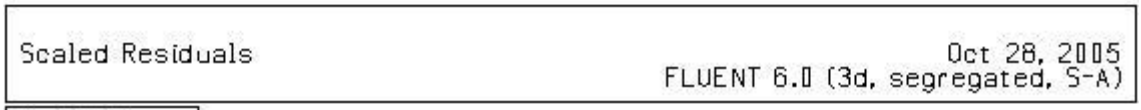
Scaled Residuals
Oct 28, 2005
FLUENT 6.0 (3d, segregated, S-A)

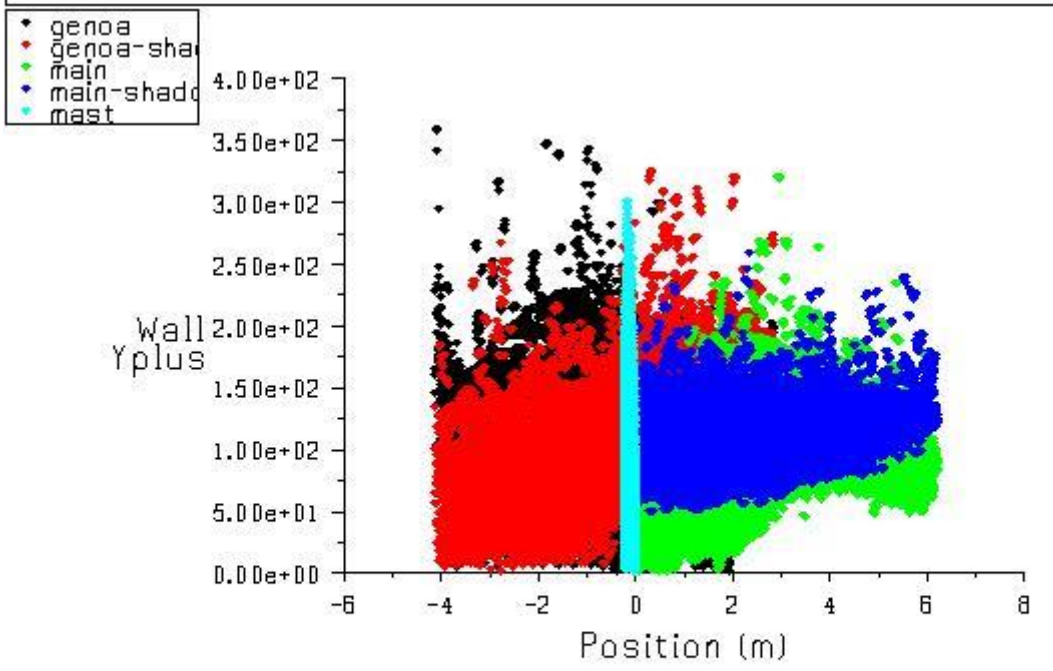
genoa
genoa-sha
main
main-shadc
mast
4.00e+02
3.50e+02
3.00e+02
2.50e+02
2.00e+02
1.50e+02
1.00e+02
5.00e+01
0.00e+00
Wall Yplus
-6
-4
-2
0
2
4
6
8
Position (m)


Wall Yplus
Oct 28, 2005
FLUENT 6.0 (3d, segregated, S-A)

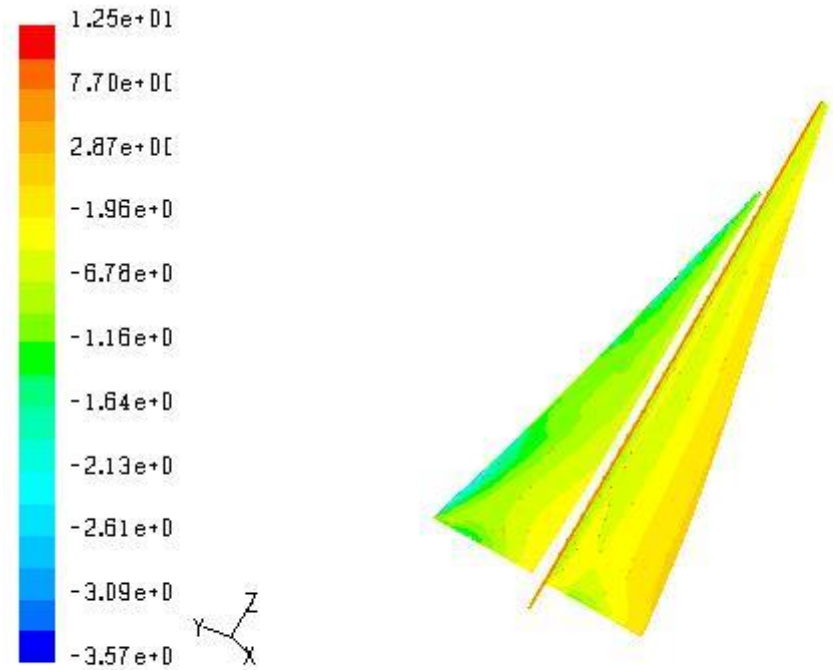

Contours of Static Pressure (pascal)

Oct 28, 2005
FLUENT 6.0 (3d, segregated, S-A)

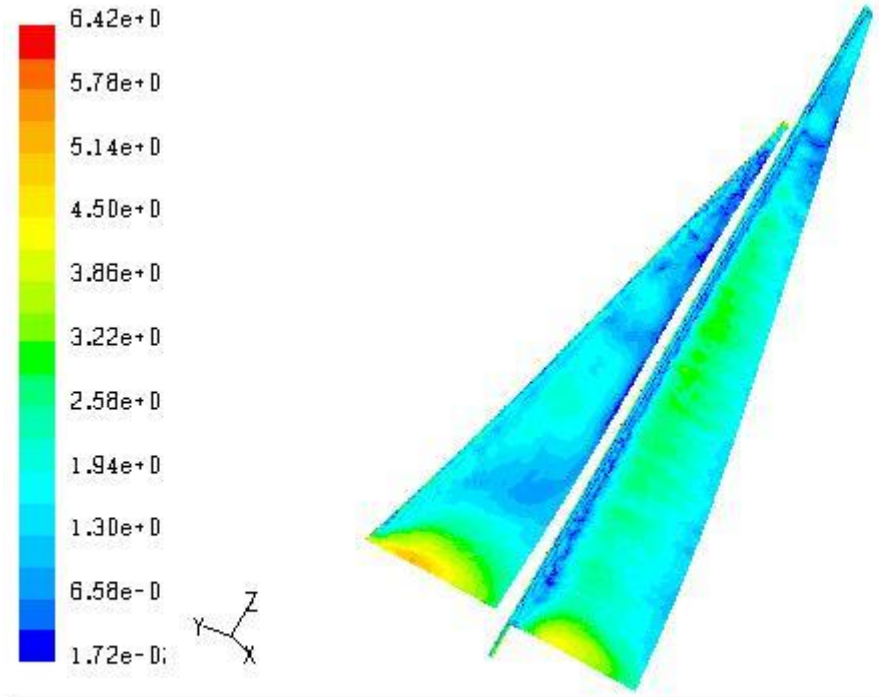

Contours of Velocity Magnitude (m/s)

Oct 28, 2005
FLUENT 6.0 (3d, segregated, S-A)

β=80 degrees

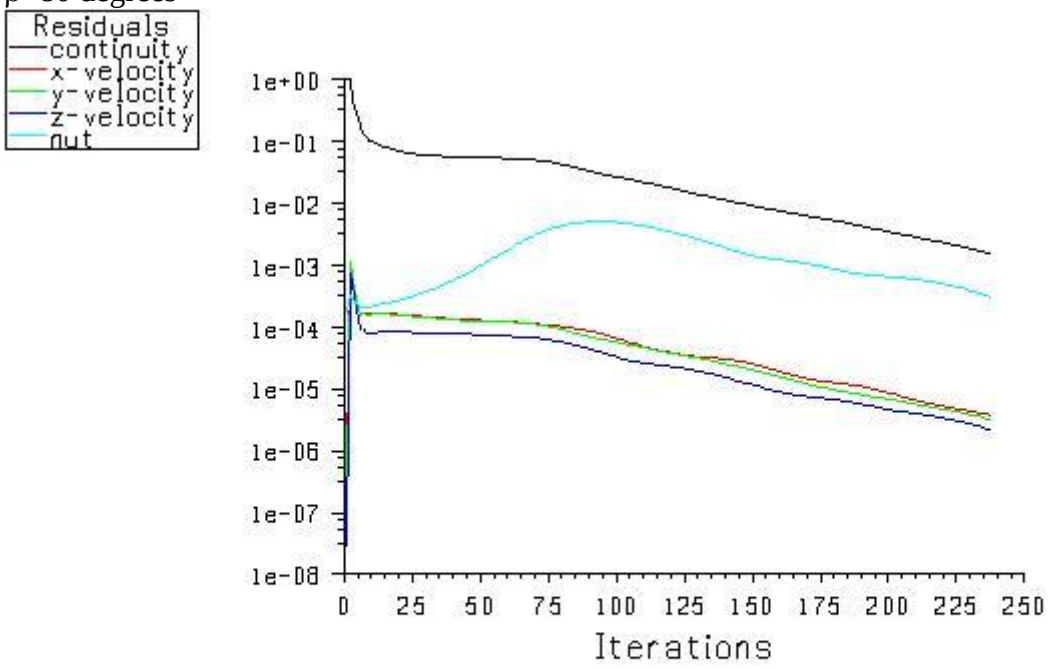
Residuals
continuity
x-velocity
y-velocity
z-velocity
nut
1e+00
1e-01
1e-02
1e-03
1e-04
1e-05
1e-06
1e-07
1e-08
0
25
50
75
100
125
150
175
200
225
250
Iterations
Scaled Residuals
Oct 28, 2005
FLUENT 6.0 (3d, segregated, S-A)

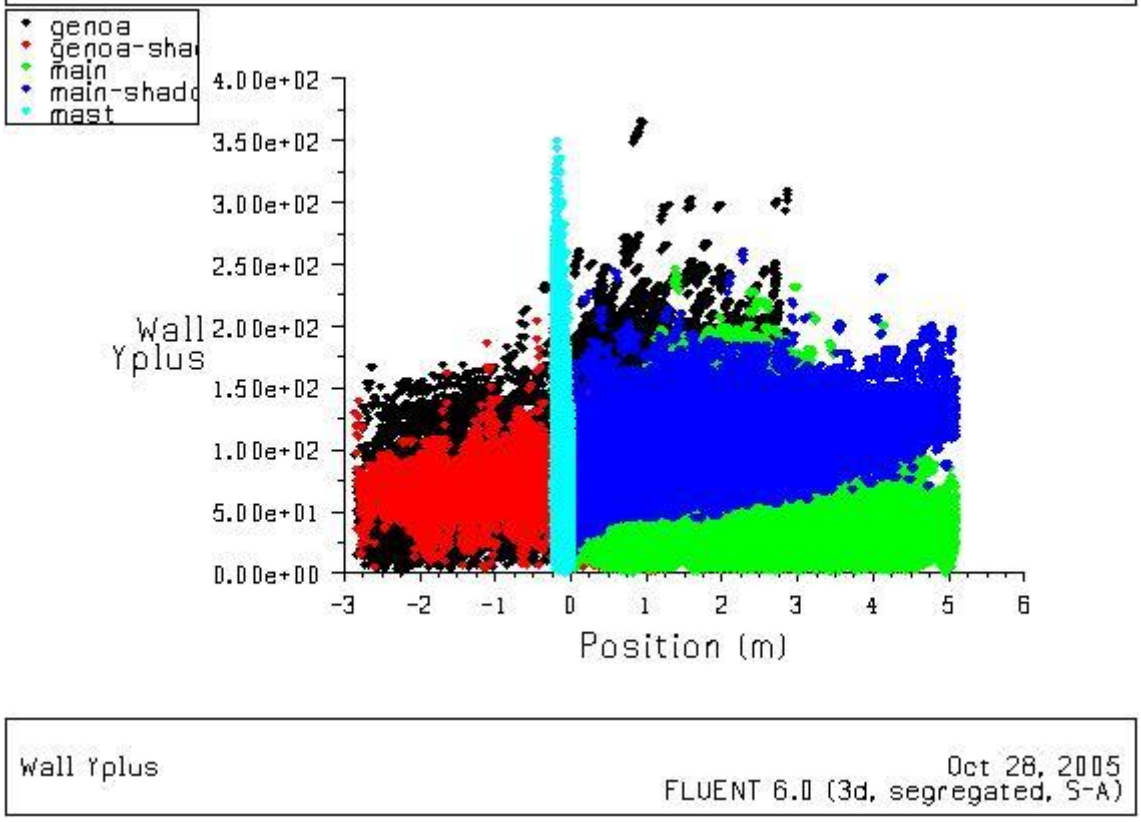
genoa
genoa-sha
main
main-shadc
mast
4.00e+02
3.50e+02
3.00e+02
2.50e+02
2.00e+02
1.50e+02
1.00e+02
5.00e+01
0.00e+00
Wall Yplus
-3
-2
-1
0
1
2
3
4
5
6
Position (m)
Wall Yplus
Oct 28, 2005
FLUENT 6.0 (3d, segregated, S-A)

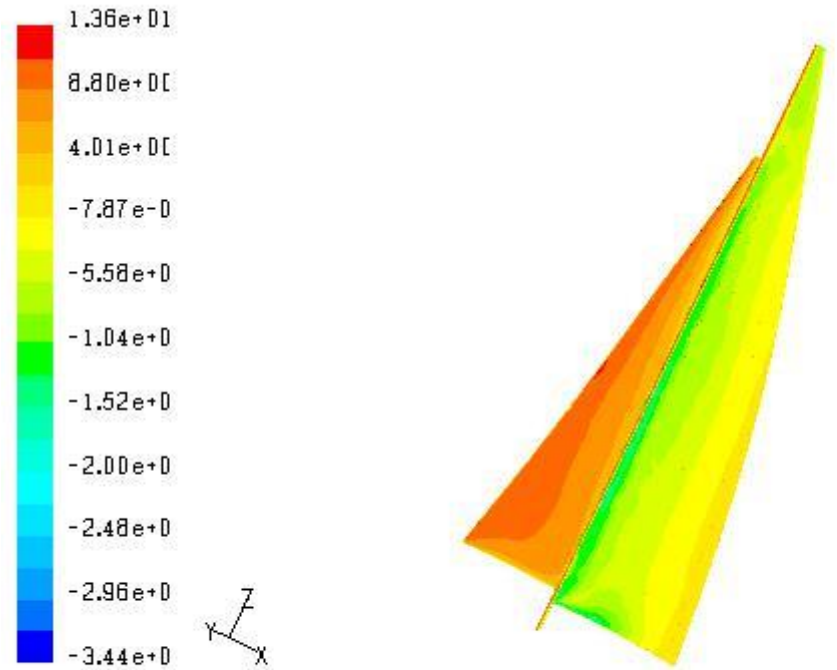

Contours of Static Pressure (pascal)

Oct 28, 2005
FLUENT 6.0 (3d, segregated, S-A)

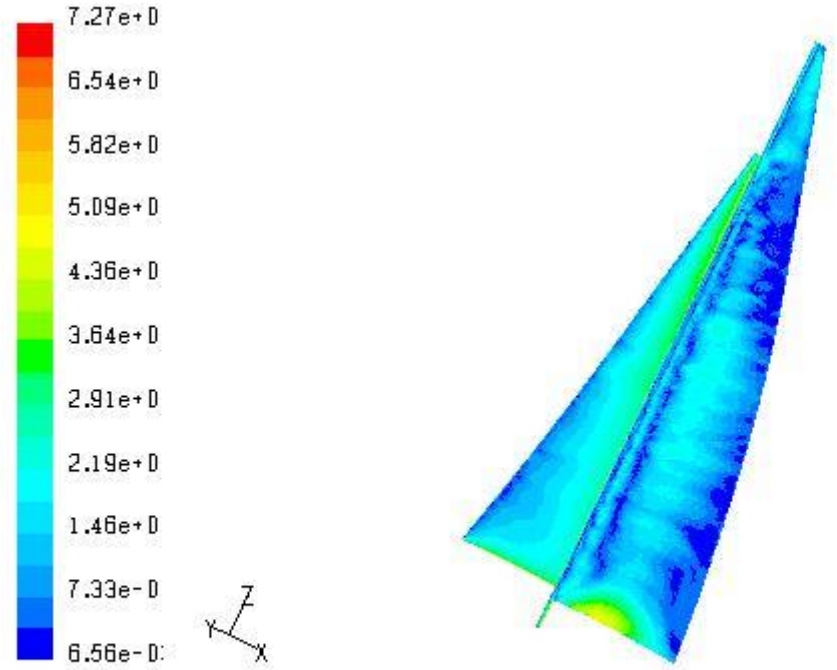

Contours of Velocity Magnitude (m/s)

Oct 28, 2005
FLUENT 6.0 (3d, segregated, S-A)